Master Thesis

Study of the log-periodic dipole antenna for the Radio Neutrino Observatory Greenland

submitted to obtain the academic degree Master of Science

Presented by

Anna Eimer

Erlangen Centre for Astroparticle Physics
Friedrich-Alexander Universität Erlangen-Nürnberg

Supervisors: Prof. Dr. Anna Nelles
PD Dr. Robert Lahmann

Abstract

Ultra high energy neutrinos can be detected via radio emission following a neutrino interaction in ice. The long attenuation length of radio signals in ice allows for a much sparser instrumentation than required for optical Cherenkov neutrino telescopes, hence making it possible to survey large volumes. The Radio Neutrino Observatory Greenland (RNO-G) is a project that will eventually consist of 35 stations (7 already deployed) with distances of about 1 km between neighbouring stations. Each station consists of 9 log-periodic dipole array (LPDA) antennas about 1.5 m below the ice surface, and with up to 100 m deep in-ice strings, equipped with vertically and horizontally polarised dipole antennas.

Understanding the antenna properties and potential interferences between nearby antennas is important to operate the experiment, to evaluate the recorded data and reconstruct neutrino properties. In this thesis, the LPDA setup was simulated with the second version of the numerical electromagnetics code (NEC2). From the simulation results the conclusion can be drawn that other antennas in close proximity influence the radiation properties of the antenna. Complementary experimental tests confirmed that the effect is negligible.

Contents

1 Introduction **1**

2 Antenna theory **3**
2.1 Radiation patterns . . . 3
2.2 Efficiency, VSWR and gain . . . 5

3 Radio detection of neutrinos and the Radio Neutrino Observatory Greenland **7**
3.1 Signal generation . . . 7
3.2 Station outline . . . 9
3.3 Signal detection . . . 10
3.3.1 Cylindrical dipole antenna . . . 11
3.3.2 LPDA antenna . . . 13

4 NEC2 simulations **17**
4.1 Numerical Electromagnetics Code (NEC) . . . 17
4.2 NEC2 antenna model . . . 18
4.2.1 Dipole design . . . 18
4.2.2 Boom design . . . 20
4.2.3 Front and rear end adjustments . . . 21
4.3 Comparison to antenna instruction manual . . . 21
4.3.1 NEC2 calculated VSWR . . . 21
4.3.2 NEC2 produced radiation pattern . . . 22
4.4 Simulation for three antennas next to each other . . . 24
4.4.1 Frequency dependency . . . 25
4.4.2 Spacing dependency . . . 27
4.4.3 Rotation dependency . . . 30
4.5 NEC2 simulation results . . . 32

5 Radio chamber measurements **33**
5.1 Radio chamber setup . . . 33
5.2 Cable and biconical antenna transmission study . . . 36
5.3 Transmission from biconical antenna to Vpol antenna . . . 39
5.3.1 Reflection calculation . . . 39
5.3.2 Waveform and distance variation . . . 41

5.3.3 Variation of number of sine oscillations 43
5.4 Radio chamber measurement results 45

6 Experimental hall measurements **47**
6.1 Experimental hall setup 47
6.2 Measurement signal and uncertainties 48
6.2.1 LPDA received signal 48
6.2.2 Statistical uncertainties 50
6.2.3 Systematic uncertainties 51
6.2.4 Sanity check 56
6.3 One LPDA radiation patterns 57
6.4 Three LPDAs next to each other 60
6.4.1 Three LPDAs in free space 60
6.4.2 Three LPDAs near wall 63
6.4.3 Result comparison to power calculation 66
6.5 Experimental hall measurement results 67

7 Conclusion **69**

A Station surface layout **71**

B CLP5130-2 geometry **73**

C Complete three antenna simulation data set **77**

D Cable reflection peaks for different frequencies **81**

1 Introduction

Neutrinos are very light, uncharged, abundant particles, barely interacting with matter. Neutrinos can be produced artificially on earth as a byproduct of nuclear power plants or at particle accelerators. They are also produced in the atmosphere via hadron decay in air showers. Other neutrino production sources can be found in outer space, for example in the sun and other stellar objects. Since they rarely interact with matter and exclusively via weak interaction, it is certain that neutrinos arriving at earth point directly back to their source. Because of this importance for multi-messenger astronomy, huge facilities with large instrumentation volumes, for example Super-Kamiokande [1] or the Cubic Kilometre Neutrino Telescope (KM3NeT) [2], and many more, were built to observe just a few events per year.

A very successful way to detect neutrinos is in ice, IceCube [3] is a very good example, which uses Cherenkov light detection. At the South Pole are also radio detection experiments for neutrino research located, such as Antarctic Ross Ice-Shelf ANtenna Neutrino Array (ARIANNA) [4] or the Askaryan Radio Array (ARA) [5]. This technique can be used to detect ultra high energetic ($\sim 10\,\mathrm{PeV}$) neutrinos, originating from cosmogenic sources. The radio detection idea is also used by the Radio Neutrino Observatory Greenland (RNO-G), currently under construction. The radio detection mechanism is based on the Askaryan effect, which will be explained in chapter 3 along with the RNO-G experiment.

In order to correctly interpret the signals obtained by the antennas, they need to be well understood. A theoretical introduction about the antennas will be given in chapter 2. Therefore, questions about the mutual influence of antennas must be answered. Although all antennas are in receiving mode, first measurements from Greenland suggest that they show interference. This question will be answered in the context of this thesis for the RNO-G project. In particular the log-periodic dipole antennas close to the surface are considered. It is a valid question, because the antenna using projects ARIANNA and the LOw Frequency ARray (LOFAR) [6] have already proven that there are a some aspects to consider.

The ARIANNA project performed surface reflection studies [7]. With antennas slightly below the ice surface two signals belong to one event, the direct signal and one signal reflected by the surface. It is crucial that both signals can be distinguished in order to reconstruct the arrival direction and hence the energy of the neutrino.

At LOFAR the simulated horizontal gain and the measured gain did not match [8]. It has been shown that cross talk occurs between the inner stations, due to the close spacing between the antennas. That has to be considered in the analysis for the LOFAR project now.

In general, the big question is when exactly no interference between the antenna signals can be expected. Theory predicts that at least a distance of two times the size of the antenna squared per wavelength is required to exclude interference, but experiments show that already smaller distances are sufficient. In this context it is interesting to see whether simulations can help to identify antenna effects or whether they are too sensitive compared to reality. The results of the simulation will be shown in chapter 4.

The goal of this thesis is to investigate reflection and interference problems for RNO-G and to determine if there is sufficient spaceing between the antennas. This should be achieved by looking at the theory, simulations, using the NEC2 simulation software [9], for the particular antenna, and measurements with different actual RNO-G antennas. Measurement results will be described in chapter 5 and chapter 6.

2 Antenna theory

For a better understanding of the terminology used in this thesis, some of the most important antenna theory terms will be explained at the beginning. This includes the term radiation pattern (see section 2.1) and associated concepts, like lobes, beamwidth and the field regions around an antenna. In addition, terms such as efficiency, voltage standing wave ratio (VSWR) and gain will be defined (see section 2.2). This chapter follows the theory presented in [10].

2.1 Radiation patterns

A *radiation pattern* is the spatial distribution of a quantity that characterises the electromagnetic field generated by an antenna [11]. Such characterising quantities could be for example power flux density, radiation intensity, field strength, directivity, phase or polarisation [10]. Most of the time, the field pattern, i.e. the magnitude of electric or magnetic field as function of solid angle, is plotted linearly, as shown in Figure 2.1. The power pattern which is the squared magnitude of the electric or magnetic field as a function of solid angle is usually plotted logarithmically or in decibel. Both types are mostly normalised with respect to their maximum value.

Besides the radiation pattern there is also the receiving pattern, which characterises the antennas sensitivity towards an incoming electromagnetic field. In most cases, this is more convenient to measure. The radiation pattern shows the conversion of a voltage into an electric field, while the receiving pattern depicts the conversion of an electric field into a voltage. This means that, both patterns describe the same conversion. Hence, the radiation and the receiving pattern are the same, which is called *reciprocity*.

The different parts of the radiation pattern are called *lobes* or *beam*. Different types of lobes are shown in Figure 2.1. There are two main categories, the major and the minor lobes. The radiation lobe, which contains the direction of maximum radiation is referred to as major lobe or main beam. Undesired minor lobes can be, for example side lobes, which point in other directions than the intended main lobe, or back lobes, which face the exact opposite direction as the main beam.

The *beamwidth* is defined as the angular separation between two identical points on the opposite side of the pattern maximum. This parameter is used to consider the trade-off between the side lobes and the width of the main lobe. There are several different ways to measure the beamwidth, two of the most frequently used definitions can be seen in Figure 2.1. The First-Null BeamWidth (FNBW) describes the opening angle of the major lobe. The beamwidth can also be described by the angle between the points where the intensity has a certain value. The most often used is the Half-Power BeamWidth (HPBW), which describes the angle between the two points where the power is one half of the maximum radiation intensity. This particular definition holds information about the antenna resolution. That is, if two radiation sources are further than the beamwidth of the antenna apart, they can be distinguished.

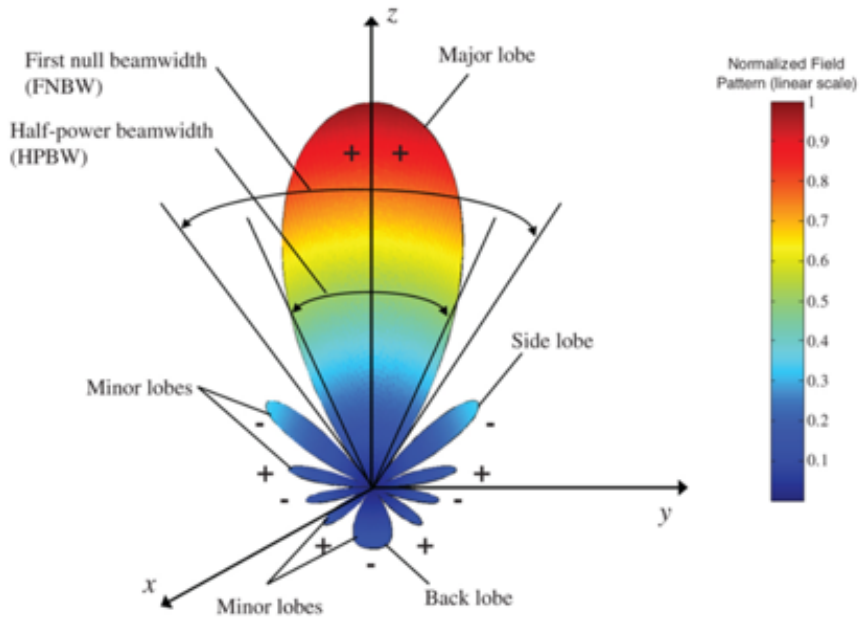

Figure 2.1: *Normalised antenna field pattern in linear scale, with denoted lobes and beamwidths. The plus and minus signs refer to the relative polarisation of the amplitude between various lobes. (Figure taken from [10])*

The antenna performance is often described in terms of its principal E- and H-plane patterns. The E-plane contains the electric-field vector and direction of maximum radiation, the H-plane contains the magnetic-field vector plane. Often the coordinate system is chosen such that one of the planes coincides with one of the geometric planes of the antenna. Since E- and H-plane are perpendicular to each other, this information can be used to derive both the *vertical* and the *horizontal plane* and therefore the three-dimensional radiation pattern.

There are three different *radial zones* around the antenna, the reactive and the radiating near field and the far field. The extent of each zone depends on the largest physical antenna dimension D and the wavelength λ. The reactive near field $r_{\text{react. n. f.}}$ is located directly around the antenna. The radiating near field $r_{\text{rad. n. f.}}$, also called Fresnel region, is situated between the reactive near field and the far field. In this zone, radiation fields predominate, and the angular field distribution depends on the distance from the antenna. The more important far field or Fraunhofer region $r_{\text{f. f.}}$ is the region of the field where the angular field distribution is independent of the distance. The following equations give a rule of thumb for the radii of the respective regions around the antenna:

$$r_{\text{react. n. f.}} < 0.62\sqrt{\frac{D^3}{\lambda}}, \tag{2.1}$$

$$0.62\sqrt{\frac{D^3}{\lambda}} \leq r_{\text{rad. n. f.}} < \frac{2D^2}{\lambda}, \tag{2.2}$$

$$r_{\text{f. f.}} \geq \frac{2D^2}{\lambda}. \tag{2.3}$$

These equations only apply, if the largest antenna dimension D is large compared to the wavelength ($D > \lambda$). Usually the far field pattern is meant when talking about the radiation pattern of an antenna.

2.2 Efficiency, VSWR and gain

The *total antenna efficiency* e_0, takes into account losses at the input terminal and within the antenna structure. These losses are due to reflections, caused by mismatch between transmission line and antenna, and I^2R losses, such as conductivity and dielectric loss.

The I^2R losses can only be determined experimentally. In addition, conductivity and dielectric loss can not be determined separately. Therefore, this contribution is called antenna radiation efficiency e_{cd}. This parameter can be used to relate the gain to the directivity.

The reflection (mismatch) efficiency e_{r} can be calculated using the *voltage reflection coefficient* Γ:

$$\Gamma = \frac{Z_{\text{in}} - Z_0}{Z_{\text{in}} + Z_0} = \frac{V_{\text{r}}}{V_0}, \tag{2.4}$$

where Z_{in} is the antenna input impedance, Z_0 is the characteristic impedance of the transmission line, V_{r} is the reflected voltage and V_0 is the original voltage. Now knowing

all the parameters, the total antenna efficiency can be written as:

$$e_0 = e_{\mathrm{cd}} e_{\mathrm{r}} = e_{\mathrm{cd}}(1 - |\Gamma|^2). \tag{2.5}$$

The voltage reflection coefficient Γ can also be used to calculate the *voltage standing wave ratio* (VSWR) [10]:

$$VSWR = \frac{1 + |\Gamma|}{1 - |\Gamma|}. \tag{2.6}$$

This parameter is often applied to characterise the antenna. It is determined to show the impedance mismatch between antenna input and transmission line, as can be seen in Equation 2.4. That means regarding the efficiency, small VSWR values lead to small signal loss due to reflection. The antenna impedance is frequency-dependent and therefore the VSWR is plotted over the frequency. The frequency for minimal VSWR is called the antenna resonance frequency [12].

The *gain* G describes the ratio of the radiation intensity $U(\theta, \phi)$ in a given direction to the radiation intensity that would be produced if the input power P_{in} accepted by the antenna was radiated isotropically [11]. The corresponding equation for the gain G reads:

$$G = 4\pi \frac{U(\theta, \phi)}{P_{in}} \tag{2.7}$$

The gain depends on the direction and is related to the radiation pattern. If the direction of the gain is not stated, the direction of maximum radiation intensity is assumed [11]. Because of this direction dependency, the partial gains in vertical and horizontal direction get summed up to form the total gain.

There are two different types of gain: relative gain and absolute gain. The relative gain compares an antenna gain with that of a reference antenna. The absolute gain also takes reflection or mismatch losses e_{cd} into account.

3 Radio detection of neutrinos and the Radio Neutrino Observatory Greenland

The Radio Neutrino Observatory Greenland, RNO-G for short, is designed to detect PeV energy neutrinos via radio emission of the neutrinos in the ice of Greenland. The project is located at the Summit Station and uses two types of antennas to detect the neutrino-induced Askaryan emission. The radio signal generation (see section 3.1) and the RNO-G setup (see section 3.2) will mostly rely on the information given in [13]. The used antennas (see section 3.3) will be described following [10].

3.1 Signal generation

The radio signal from a neutrino event is produced by the *Askaryan effect*. When the neutrino interacts with the ice, it generates an hadronic and, in case of an electron neutrino, an electromagnetic shower (yellow dots in Figure 3.1). The presence of a moving uncompensated charge in a shower may increase a flash of Cherenkov, Bremsstrahlung, or transition radiation in the radio range by many orders of magnitude [14]. As indicated in Figure 3.1 the Askaryan radiation is emitted at or close to the Cherenkov angle. The emission can travel directly or on bent trajectories to the RNO-G station, depending on the profile of the index of refraction of the ice, represented by the red and purple lines in the sketch. The bent or reflected trajectories are more common in the shallow ice and the straight trajectories occur in the deep ice.

The radio signal emitted by such a process can be seen in Figure 3.2, it is a single bipolar pulse. The amplitude of the electric field waveform depends on the deviation from the Cherenkov cone. The higher the discrepancy the lower the amplitude, due to loss of coherence. Looking at the frequency spectrum for the different angles it can be seen that the Cherenkov angle shows the broadest available frequency range. Going off cone, the probability to see signals with high energies decreases. Therefore, the most probable frequency range to find a signal with RNO-G is between 100 MHz and 500 MHz.

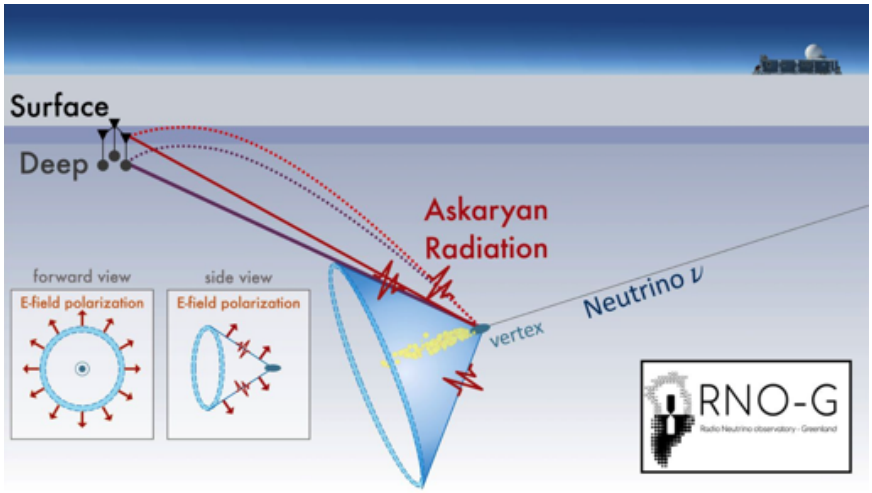

Figure 3.1: *Schematic representation of the detection of radio emission following a neutrino interaction (not to scale). The emission is strongest at the Cherenkov angle (blue cone) and can follow straight and bent trajectories to the receiving station. The signal is usually detected at large distances and is strongly polarised as illustrated in the insets. (Figure taken from [13])*

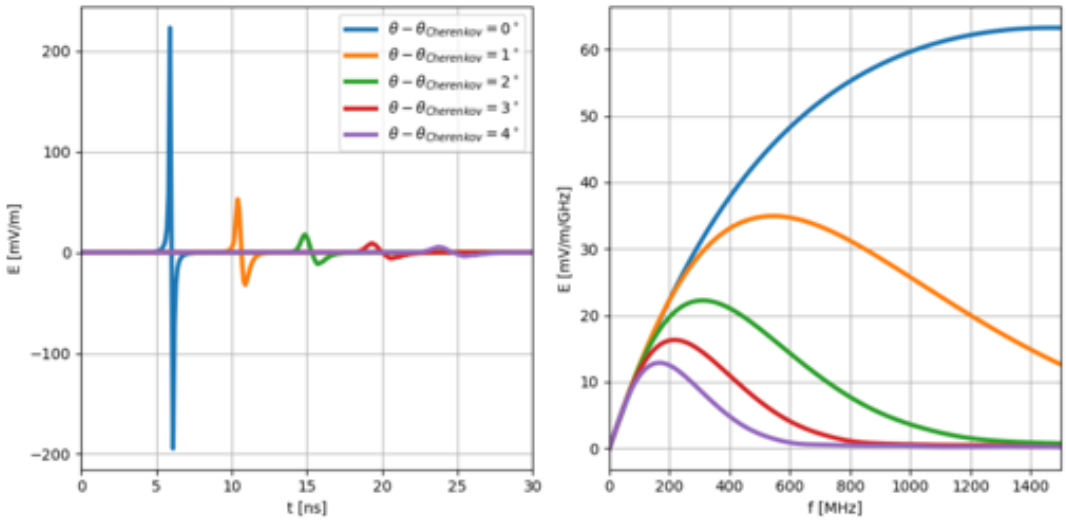

Figure 3.2: *Electric field waveforms (left) and spectra (right) of the radio signal emitted at different viewing angles relative to the Cherenkov angle, for a hadronic shower with energy deposition of* 1 EeV*. For better readability, the waveforms have been offset in time. Propagation and detector effects have not been included. (Figure taken from [13])*

3.2 Station outline

Once completed, RNO-G will comprise 35 stations on a square grid of 1 km baseline (see Figure 3.3 right), in order to detect the neutrino radio emission. RNO-G uses the facilities of Summit Station in the middle of Greenland for this project. The layout of one of the stations can be found in Figure 3.3 on the left. All the stations have a deep component and a surface component. This concept makes it a mixture of the ARIANNA (surface array) and the ARA (down-hole array) approach. Both have their own task, but observing events in the deep and in the surface component in coincidence will be especially valuable for event reconstruction.

The deep component, up to 100 m down in the ice, consists of three strings with horizontally polarised (Hpol) and vertically polarised (Vpol) antennas. The Vpol antennas are used to reconstruct the vertex and the arrival direction. The Hpol antennas improve the full electric field reconstruction. One of these strings also contains the phased array which acts as a low-power and low-threshold trigger. This string is referred to as the power string, the other two are called support strings and also contain calibration pulsers. The three independent strings are required in order to obtain azimuthal information, provided by the Vpol antennas.

The surface component, about 1.5 m below the surface, consists of 9 log-periodic dipole antennas (LPDAs). There are always three antennas grouped together. Within every group the spacing between the antennas is approximately 3 m (detailed layout in Appendix A). These are oriented in different directions, one facing upwards to the surface and two downwards into the ice at an 120° angle. This setup tries to prevent cross talk between the antennas. The different orientations are needed to gain more detection volume, and their broad-band sensitivity also widens the frequency coverage of the detector. The high frequency coverage helps determine the radio detection angle with respect to the Cherenkov cone, improving energy reconstruction and pointing resolution. This component will deliver polarisation measurements and timing information for all events. The upward facing antenna acts as an air shower veto and is intended to measure backgrounds such as tribo-electric events, weather balloons etc.

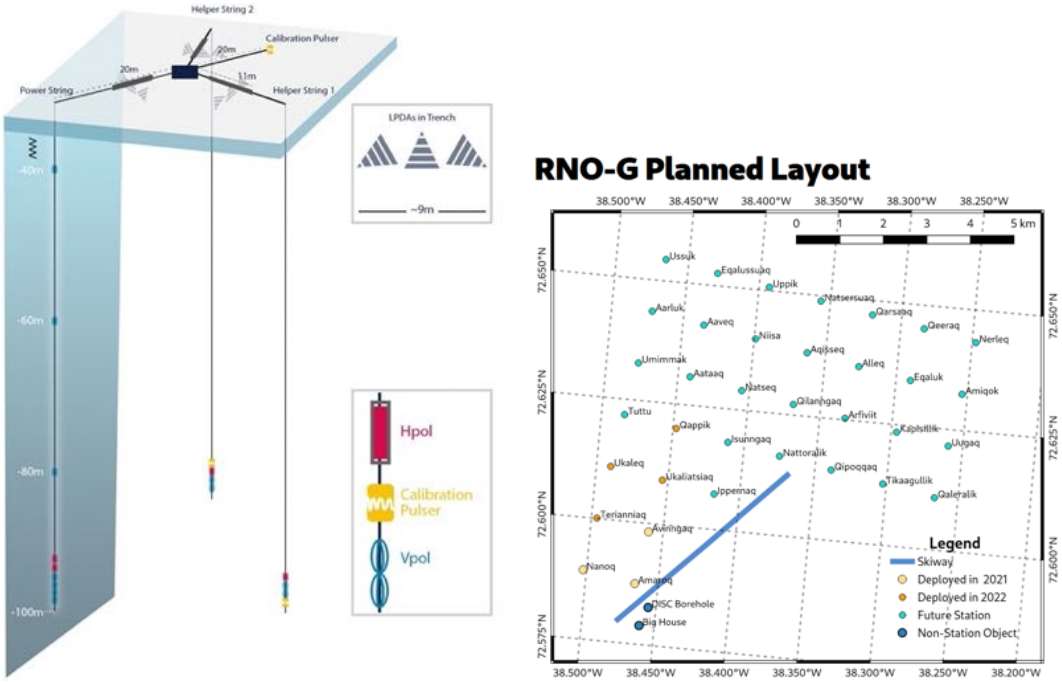

Figure 3.3: *The layout of an individual RNO-G station is shown on the left, with a deep component consisting of three strings of horizontally polarised and vertically polarised antennas, one of which contains a phased array as a trigger, and a surface component consisting of LPDA antennas. RNO-G layout with its 35 stations is shown on the right. The stations marked in yellow and orange are already deployed, the light blue stations will be built in the future. (Figure taken from [15])*

3.3 Signal detection

In order to detect these neutrino signals RNO-G uses dipole antennas and LPDAs. All the different antennas are mentioned in section 3.2. The LPDA is subject of this thesis and therefore will be explained in more detail in this chapter. In particular its design, since this is needed to create a model for the simulation, and what to expect to get for the fundamental properties from theory. Since also a Vpol antenna is used, cylindrical dipole antennas and the properties of the version used in RNO-G will also be described briefly.

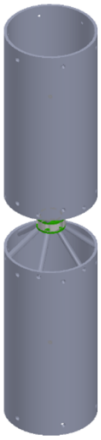

Figure 3.4: *Schematic drawing of the Vpol antenna designed for RNO-G. (Figure taken from [16])*

3.3.1 Cylindrical dipole antenna

Design Cylindrical dipole antennas have the geometry of a wire with finite diameter and length. They are a special form of the biconical antenna. Its radiation characteristics are frequency-dependent and the bandwidth can be enlarged by decreasing the length to diameter (l/d) ratio [10]. This is the reason why the dipole antennas for RNO-G are also called fat dipoles. They are designed by the collaboration especially for the purpose of RNO-G. A schematic drawing can be seen in Figure 3.4.

Properties As Figure 3.5 shows, the RNO-G Vpol antennas receive signals isotropically in the horizontal plane and are most sensitive at 400 MHz, as needed for the RNO-G experiment. The vertical gain plot over frequency shows how broadband this antenna is and that the signal amplification can be up to 4 dB. The angle scale starts at the top of the antenna, meaning 90° (boresight) corresponds to the horizontal plane. Looking at the different angle data sets, one can also tell that for frequencies below 0.45 GHz the signal gets less amplified with increasing inclination.

Another important parameter is the VSWR (see section 2.2), the corresponding data for the Vpol antenna can be found in Figure 3.6. In the frequency regime above 200 MHz, which is the relevant range for RNO-G, the VSWR has a value of 2, meaning it is small, leading to the conclusion that the signal loss due to reflections is small. Therefore, this plot shows that the fat dipole for RNO-G is very efficient.

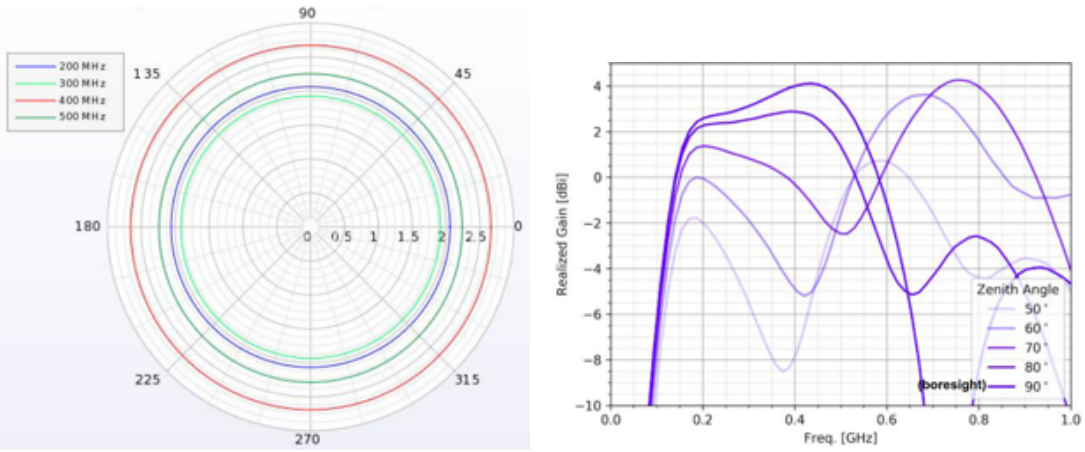

Figure 3.5: *The horizontal (azimuth) and vertical (zenith) radiation patterns of the Vpol antenna are shown on the left and right respectively. The realised gain versus frequency is shown for different angles, with 90° being at the level of the boresight. (Figures taken from [17])*

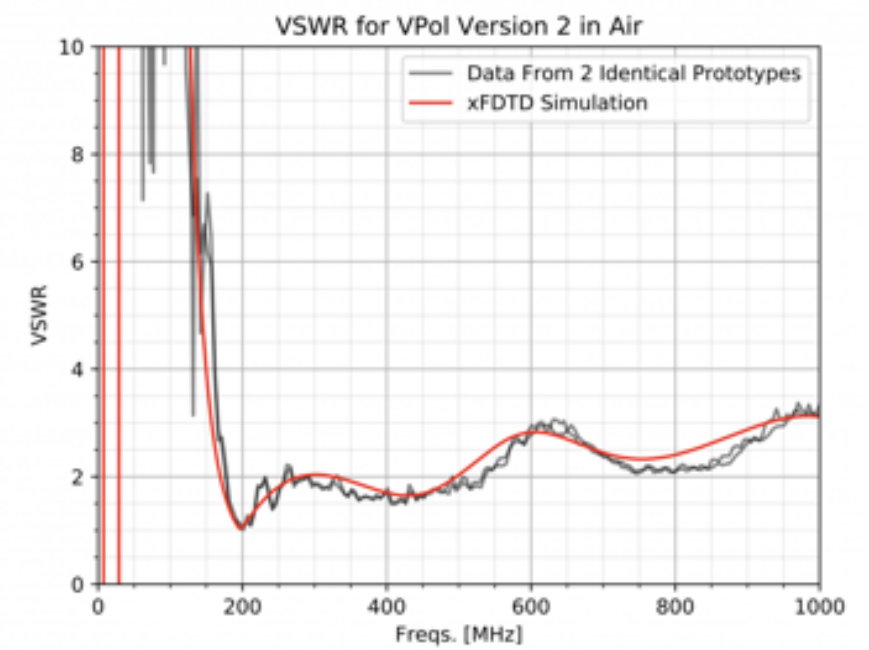

Figure 3.6: *VSWR over frequency for the second version of the Vpol in air, simulated (red) and measured (grey). (Figure taken from [15])*

3.3.2 LPDA antenna

The log-periodic dipole array or antenna (LPDA) is a so called broadband antenna, meaning it can radiate and receive a wide range of frequencies. This property is needed in order to receive signals in the frequency range discussed in section 3.1. In addition, the antenna is almost frequency-independent, the reason will be explained later in this subsection. A frequency independent antenna geometry can be completely specified by angles. The advantage of this type of antennas is their invariance to a change of physical size. So if the antenna dimensions are decreased by a factor, the frequency increases by the same amount [10].

Design The LPDA consists of a sequence of $n = 1, ..., m$ side-by-side parallel linear dipoles forming a coplanar array. The lengths (l_n), spacings (R_n), diameters (d_n), and gap spacings at the dipole centers (s_n) of the log-periodic array increases logarithmically as defined by the inverse of the *geometric ratio* τ. This leads to a range of ratio equations, given in Equation 3.1. The parameters are displayed in Figure 3.7. Typical values for τ lie between 0.7 and 0.95 [10].

$$\frac{1}{\tau} = \frac{l_{n+1}}{l_n} = \frac{R_{n+1}}{R_n} = \frac{d_{n+1}}{d_n} = \frac{s_{n+1}}{s_n} \tag{3.1}$$

Another important parameter is the *spacing factor* σ. As can be seen in Equation 3.2, it describes the distance between two neighbouring dipoles n and $n + 1$. This distance decreases with decreasing dipole lengths, but the ratio is the same for the complete array.

$$\sigma = \frac{R_{n+1} - R_n}{2l_{n+1}} \tag{3.2}$$

With these non-angle-dependent parameters, it is obvious why it is not a completely frequency-independent antenna. The dipole ends form a certain angle 2α and therefore it is almost frequency independent. Typical designs of LPDAs have *apex half angles* of $10° \leq \alpha \leq 45°$ [10]. The footpoint of this angle is called virtual array vertex (VAV) and from there to the corresponding dipole the spacing R_n is measured [12].

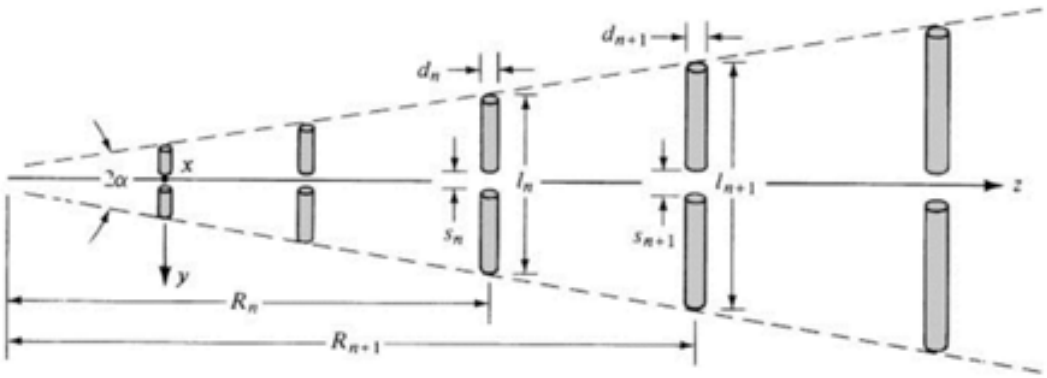

Figure 3.7: *Sketch of a log-periodic dipole array with the following parameters: angle (α), length (l_n), spacing (R_n), diameter (d_n), and gap spacing at dipole centres (s_n). (Figure taken from [10])*

The general configuration of a log-periodic dipole array is described in terms of the parameters τ (see Equation 3.1), α and σ (see Equation 3.2) related by Equation 3.3 [10], using the definitions from above.

$$\alpha = \tan^{-1}\left(\frac{1-\tau}{4\sigma}\right) \tag{3.3}$$

Since one cannot produce an infinitely large log-periodic array, not all frequencies can be deployed by one antenna. This leads to a lower frequency cutoff when the longest element length is $\lambda_m/2$. The highest frequency cutoff occurs when the shortest element is nearly $\lambda_1/2$ [10]. A rough estimate of the frequency bandwidth for the used antenna is shown in subsection 4.2.1.

The active region of the LPDA is near the elements with lengths nearly or slightly smaller than $\lambda_n/2$ [10]. The active elements are the longer ones for lower frequencies and the smaller elements receive or radiate higher frequencies. The energy from the shorter active elements travelling to the longer inactive dipoles decreases rapidly, therefore the reflected energy from the truncated ends is negligible.

Properties Typical LPDA radiation patterns can be found in Figure 3.8. The main beam is pointed in forward direction, meaning in $-z$-direction using the coordinate system shown in Figure 3.7. In some cases also small back lobes exist. As can be seen, LPDAs have a favourable focus in forward direction. These radiation patterns also show the correlation between the geometric ratio τ and the angle α. The beamwidths are nearly constant in both horizontal (E) and vertical (H) plane [18].

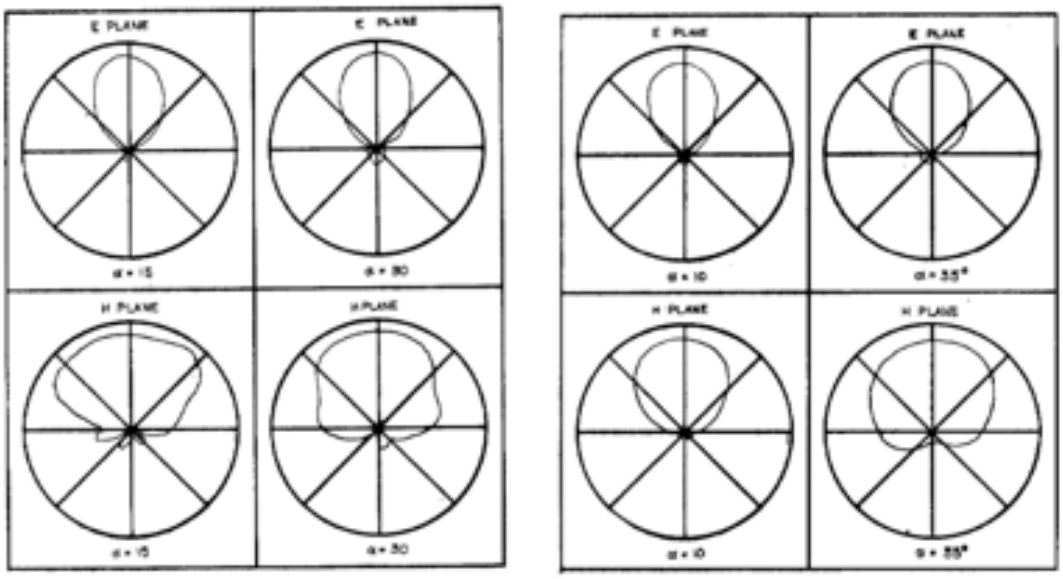

Figure 3.8: *LPDA radiation pattern sketches for $\tau = 0.81$ (left) and $\tau = 0.89$ (right). The upper pictures show the E-plane (horizontal) and the lower pictures the H-plane (vertical). For $\tau = 0.81$ the patterns are shown for $\alpha = 15°$ (outer left) and $\alpha = 30°$ (inner left). For $\tau = 0.89$ the patterns are shown for $\alpha = 10°$ (inner right) and $\alpha = 35°$ (outer right). Presumably, the patterns are plotted on a logarithmic scale (not indicated in the reference). (Figure taken from [18])*

The VSWR (see section 2.2) for LPDAs in a frequency range between 50 MHz and 1500 MHz is always between the values 1 and 2. Those low values suggest that the signal loss due to reflections for these antennas is small. For the plots in Figure 3.9 a commercial LPDA was used with an overall length of 105 in (266.7 cm) and a size of 122 in (309.88 cm) for the longest dipole, described by [10]. The statement in these plots holds true for most of the log-periodic dipole antennas. The upper part of this figure shows that the VSWR has several minimas, corresponding to antenna resonance frequencies.

Another important parameter for the LPDA characterisation is the gain. It is displayed in the lower part of Figure 3.9 for the commercial LPDA, explained in the previous paragraph. The gain increases with increasing frequency. This leads to the conclusion that one should obtain better or stronger signals at higher frequencies and therefore more signal power. At the relevant range for radio neutrino signals, above 100 MHz, the gain is already about 6 dB, meaning the signal amplitude already doubles in size.

All these parameters help to verify results delivered by the simulations and the measurements. It provides a good orientation, but since the deviation from one antenna to the other can be large, they need to be looked at critically.

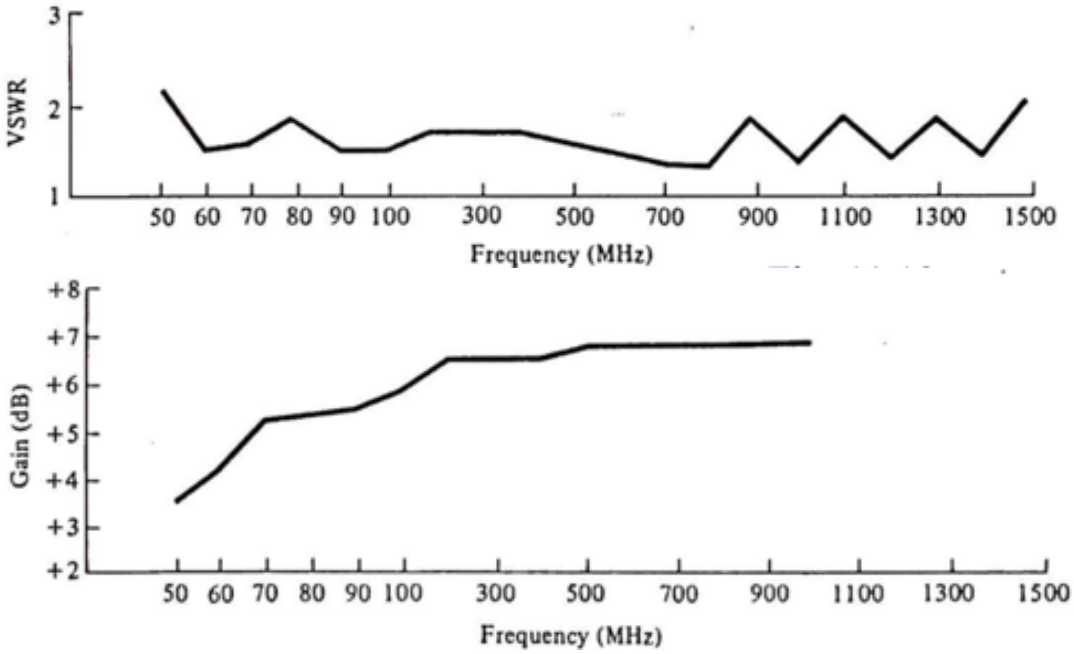

Figure 3.9: *Properties of a commercial log-periodic dipole array. The upper plot shows VSWR over frequency and the lower plot shows gain over frequency. (Figure taken from [10])*

4 NEC2 simulations

In order to gain some knowledge about the antenna response and what to expect from the measurements, simulations had to be made. Therefore the LPDA CLP5130-2 used for RNO-G (see Appendix B and [19]) was modelled with a NEC2 based simulation software (see section 4.2). Radiation patterns in different configurations were produced and analysed.

4.1 Numerical Electromagnetics Code (NEC)

The Numerical Electromagnetics Code (NEC2) is a user-oriented computer code for the analysis of the electromagnetic response of antennas and other metal structures [9]. It uses the numerical solution of the electric-field and the magnetic-field integral equations, in order to model near and far field patterns and some other antenna characteristics. The field equations are evaluated using the moment method.

According to [9] the programm works without any simplifications, i.e. the problem is solved as precise as the physics can be described with the given equations. Therefore, modelling errors should be minimal. Nevertheless the system is prone to numerical errors. The biggest error source will be inaccurate inputs about the antenna geometry.

NEC2 has some practical features, needed for this project. It can model excitation in form of voltage sources and incident plane waves. The code is also able to simulate different types of ground, from ideal ground to very realistic ground using the Sommerfeld-Norton method, and reveal how they influence the field patterns. The most important aspect for this thesis is the ability to duplicate antenna structures and simulate the influence of these copies on the main antenna.

Due to the public availability, the second version of the numerical electromagnetics code, called NEC2, was used in this thesis. Specifically, the Windows implementation 4nec2 was used. The provided graphical interface has a lot of easily accessible options, making it very convenient to use.

4.2 NEC2 antenna model

The antenna parameters discussed in subsection 3.3.2 are now used to create a model of the LPDA CLP5130-2[i]. A picture of the real antenna is shown in Figure 4.1. In order to model the LPDA correctly, the dipoles, the boom (transmission line between the dipoles), and the front and rear end had to be specified. The antenna material was not considered for the simulation.

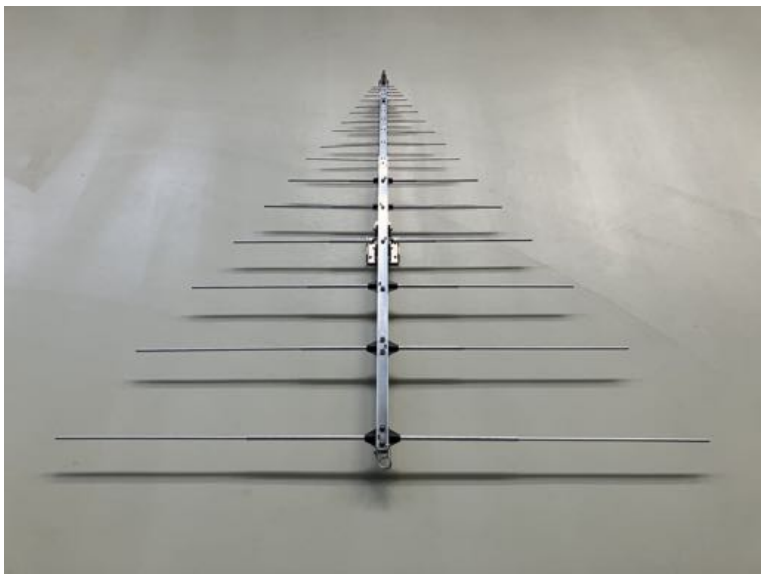

Figure 4.1: *Photograph of the used CLP5130-2 LPDA antenna. On the upper side, in front of the shortest dipole, is the feeder point for the voltage source. On the lower end of the antenna, after the longest dipole, there is a small coil. The mounting structure for the antenna is located around the fourth longest dipole in order to balance it.*

4.2.1 Dipole design

The τ parameter was calculated using the 17 dipole lengths l_n for Equation 3.1, and checked with the dipole distances R_n, both can be found in Appendix B. The maximal dipole length l_{max} is 1.45 m, as can be found in the antenna manual provided by the manufacturer [19]. The minimal dipole length l_{min} was measured to be 0.078(3) m. For this antenna $\tau_{\text{meas}} = 0.833(7)$. Comparing τ values to the theoretical range from 0.7 to 0.95 (see subsection 3.3.2), the calculated τ value seems reasonable.

Measuring also the distances between the dipoles R_n, the ratio σ_{meas} is 0.083(3). This leads to a gain of the antenna between 6.5 dB and 7 dB, as can be seen in Figure 4.2. As

[i] model available on the RNO-G GitHub page in the LPDA_analysis repository

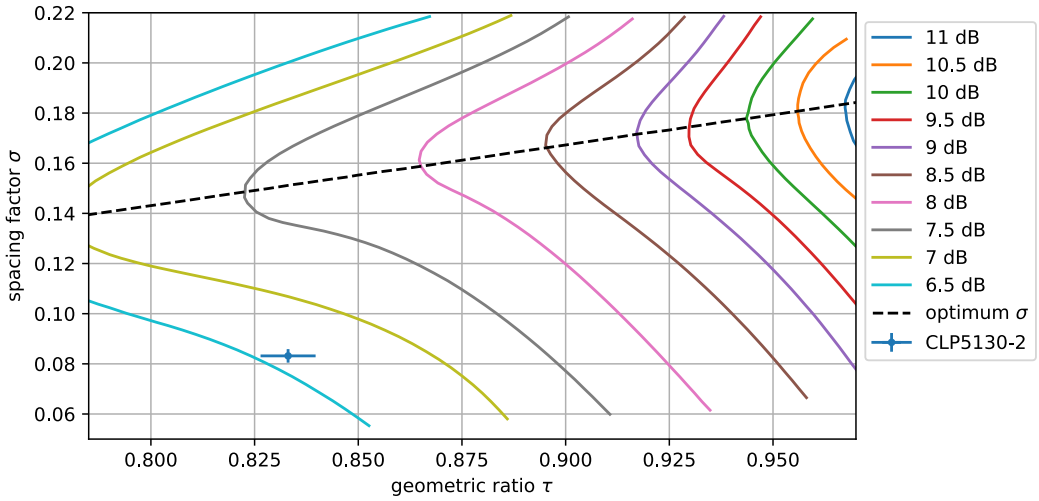

Figure 4.2: *Relation between the parameters σ and τ and the resulting gain. The plot also contains the line of optimal sigma for a certain τ. (These features of the graphic originate from [10], digitised with [20]). The data point shows the result of the measured CLP5130-2 LPDA antenna parameters.*

a result there is a discrepancy between the measurements and the instruction manual, predicting gain values from 7 dB to 8 dB. According to Figure 4.2, these parameters are not optimal, since they are located far from the optimum σ line. But with an apex half angle of $\alpha_{\text{meas}} = 26.6(7)°$ and the discussed τ_{meas} value, the antenna parameters are still within the theoretically expected values (see subsection 3.3.2).

Two different diameter d_n were chosen for the dipoles. This simplification was made because of practicability and is not in accordance with the theory from Equation 3.1. One diameter is used for the smaller already fully constructed dipoles, dipoles 1 to 11, and one for the bigger dipoles, which had to be assembled by the user, visible by the black connection between dipole and boom (see Figure 4.1). The smaller dipoles have a diameter of 4.1 mm and the bigger ones a diameter of 7 mm. These exact values were suggested by the 4nec2 software, as commonly used diameters, and match the measured radii.

With the lengths l_{max} and l_{min} the minimal frequency f_{min} and maximal frequency f_{max} can be checked by Equation 4.1, where c is the speed of light [12]. The calculated f_{min} of 103 MHz and f_{max} of 1282 MHz fit very nicely to the manufacturer specifications of 105 MHz to 1300 MHz [19].

$$f_{\text{min}} \approx \frac{c}{2l_{\text{max}}}, \qquad f_{\text{max}} \approx \frac{c}{3l_{\text{min}}} \tag{4.1}$$

4.2.2 Boom design

Besides the dipoles also the boom needs to be implemented into the model. The term boom is used for the part connecting the dipoles with each other and with the connector. In the case of the CLP5130-2 the boom is a coaxial connection. This feature was implemented by using a crisscross transmission line (see Figure 4.3, blue crosses in the middle) with transmission line impedance $Z_0 = 105\,\Omega$. This value was extracted from the LPDA design tool [21] (see Appendix B). Using a VSWR of 2, an input impedance Z_{in} of $50\,\Omega$ and a combination of Equation 2.4 and Equation 2.6, a similar value could be derived[i].

The advantage of a crisscross connection in contrast to a straight connection is the negligible interference effects. Through the crisscrossing a 180° current phase is introduced and therefore very little energy is radiated between the closely spaced short elements [10].

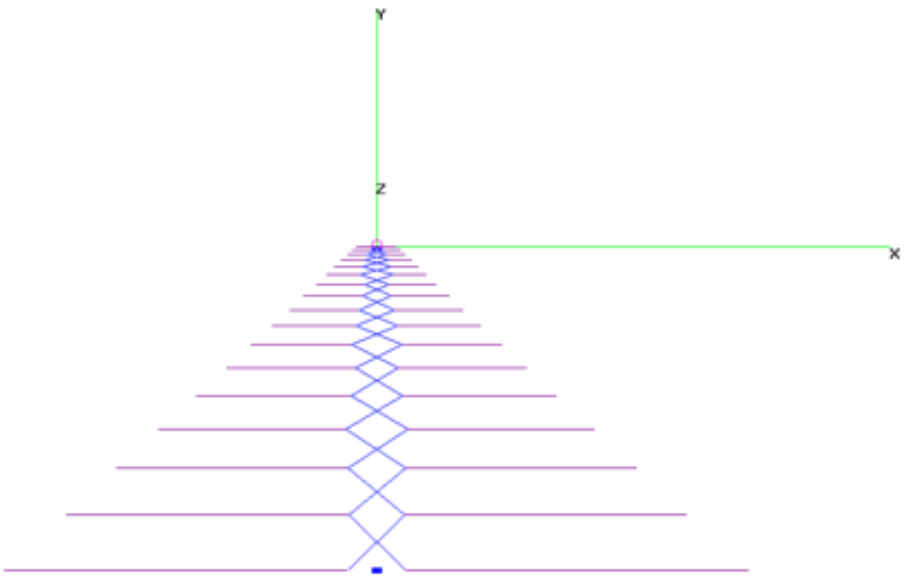

Figure 4.3: *Model of the transmitting CLP5130-2 LPDA in the NEC2 simulation software 4nec2. The coordinate system is given in green with z pointing in upward direction. The dipoles are depicted as purple lines. The boom is displayed as blue crisscross transmission line connecting all the dipoles in the middle of the construction. The pink circle marks the front end voltage source and the blue rectangle the rear end coil.*

[i] calculation available on the RNO-G GitHub page in the LPDA_analysis repository

4.2.3 Front and rear end adjustments

At the front end, in the middle of the first dipole the voltage source was placed for the emitting antenna. In order to make it comparable to the actual measurements the voltage was chosen to be 250 mV, unless stated otherwise. For the receiving antenna a resistance of 50 Ω was placed at this position.

In addition to the standard parts of an LPDA, in this case also a small coil at the rear end of the antenna had to be implemented. After measuring the physical dimensions an inductance of 0.8 H was used for the simulations.

Both features can be seen in Figure 4.3. Note that in this figure a transmitting antenna is displayed and therefore the pink circle represents the voltage source. The blue rectangle indicates the coil.

4.3 Comparison to antenna instruction manual

In order to further validate the model described in section 4.2, parameters given in the instruction manual [19] were used. In the following section the VSWR and the radiation pattern of the model will be compared to the manual.

4.3.1 NEC2 calculated VSWR

One characteristic that was specified by the manufacturer that could be used for a validity check is the voltage standing wave ratio (VSWR). In Figure 4.4 a qualitative comparison of the simulation results and the instruction manual graph is given. Apart from three major outliers, the typical value of about 2 (see section 2.2) for the VSWR seems to be given in the simulation.

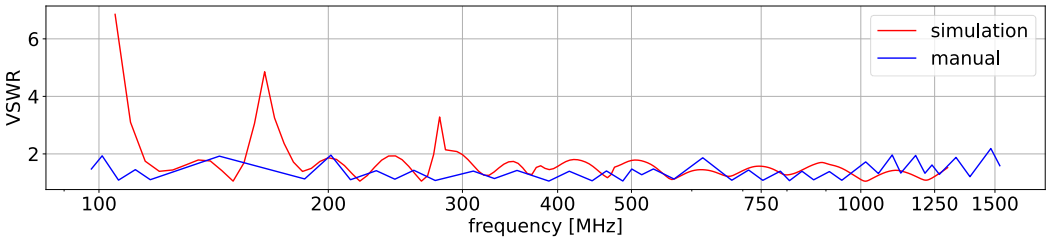

Figure 4.4: *VSWR comparison of the simulation (red) and the instruction manual (blue, see [19], digitised with [20]).*

A quantitative comparison with the instruction manual data does not seem advisable, as the curves data points appear to be the minima and maxima connected by lines. Only a few data points are comparable. There is also no further explanation of this data or an uncertainty estimation. Nevertheless a quantitative analysis proves the model to meet the VSWR requirements of the used antenna.

4.3.2 NEC2 produced radiation pattern

To check whether the designed model behaves like the real antenna, the radiation pattern from the antenna instruction manual was used. The results can be seen in Figure 4.5. This check was carried out at 300 MHz for free space, meaning no ground corrections were implemented.

In Figure 4.5 the radiation pattern for the horizontal (dashed line) and the vertical (solid line) plane are shown on the left side as depicted in the instruction manual [19], and the right side displays the simulation results for 300 MHz. The origin of the angle scale was used to display the point of maximum radiation, corresponding to the feed point of the LPDA. The decibel (dB) scale was used and each pattern was normalised to be 0 dB at the maximum radiation point. It seems that the instruction manual plotted the already dB radii again in a logarithmic scale. The simulation plot also includes the half-power points, in case of the dB scale, located at a radius of −3 dB. These are used to find the half-power beamwidth (HPBW), meaning the angle where most of the power is radiated.

The dashed horizontal patterns in Figure 4.5 look similar. Both have the same structure, a big major lobe and a small back lobe. The difference lies in the ratio between the lobes. The back lobe in the manual pattern is always below −20 dB, whereas the back lobe in the simulation surpasses −20 dB slightly. Therefore in the simulation more radiation is emitted in backwards direction, but since the scale is logarithmic, both back lobes have a small effect compared to the major lobe.

The vertical radiation patterns, solid lines in Figure 4.5, have almost the same shape. Both patterns look like a sphere which is cut in the back. This asymmetric shape shows that the antenna is more sensitive in forward direction than in a backwards direction, as expected. The instruction manual pattern is a bit more rounded than the simulated pattern.

Comparing these patterns to the theoretical shapes shown in Figure 3.8 they look very similar. All horizontal patterns have a large major lobe and one small back lobe. The similarities of the vertical patterns is even better, the shape of the simulated and theoretical patterns match very well. This also leads to the conclusion that the model describes an LPDA.

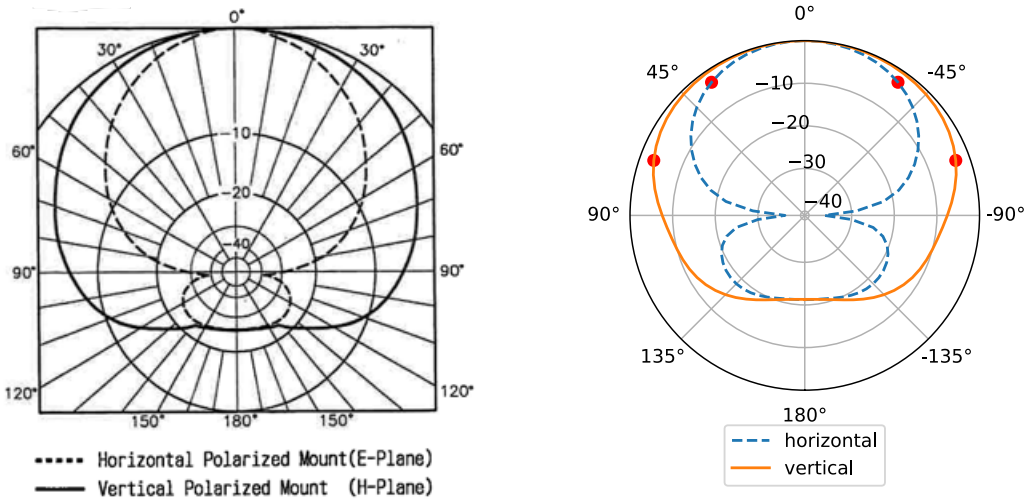

Figure 4.5: *Comparison of the free space horizontal (dashed line) and vertical (solid line) radiation pattern of the simulation (right plot) and the instruction manual [19] (left plot) for the CLP5130-2 LPDA antenna. For all patterns the radius is plotted in* dB *and is normalised in a way that the maximum gain is* 0 dB*. The red dots represent the half-power points.*

The calculated half-power beamwidths[i] can be found in Table 4.1. The values for the instruction manual patterns were given in the specifications [19]. For the simulation the HPBW was calculated searching for the nearest radii around −3 dB in each half of the pattern and adding up the corresponding angles to get the full HPBW. Comparing these results to the specification values given in the manual, the simulation is meeting the expectation. The discrepancy in radiation pattern and beamwidth between manual and simulation could be due to errors in the model.

	vertical	horizontal
simulation	140.0	70.0
specification	130 ∼ 110	70 ∼ 60

Table 4.1: *Beamwidth angles in degree for the data taken from the manual radiation pattern plot (manual), the radiation pattern plot from the simulation, and the printed specifications.*

[i] calculation available on the RNO-G GitHub page in the LPDA_analysis repository

4.4 Simulation for three antennas next to each other

In a RNO-G station, three antennas are grouped together in close proximity (antennas positioned equidistantly along a straight line with length of approximately 9 m), therefore the influence on the radiation pattern has to be studied. For this purpose different distances and different radiation frequencies (100 MHz, 400 MHz, 800 MHz and 1200 MHz) were used. These frequencies were chosen to investigate the full frequency spectrum of the LPDA. Considering the results calculated in subsection 4.2.1, 100 MHz is slightly below the 105 MHz boundary of the LPDA. Still, the simulations with this frequency provide plausible results.

In the simulation, one antenna radiates a 250 mV signal (left antenna with pink circle at the top in Figure 4.6), when there are two passive antennas (middle and right antennas with blue rectangles at the top) to its right side[i]. Two examples of simulated configurations are shown in Figure 4.6.

The left configuration shows the starting point: three antennas perfectly aligned next to each other. This alignment was used to test different distances between the antennas. The distances were 1.5 m to place them as tightly together as possible, 2 m, slightly less than the closest configuration used in a RNO-G station, 3 m, the currently average configuration used at RNO-G, and 4 m to see what happens when they are further apart. The simplified setup was used because the actual RNO-G setup, described in section 3.2, was not realisable in the simulation framework.

The right-hand side shows the configuration twisted as much as possible, to study x and y rotation effects. The antenna in the middle is facing in the opposite direction than the other two, and all antennas are slightly rotated with respect to each other. Due to the copying limitations of the NEC2 simulation programme, the second copied antenna is only shifted and not rotated by 30° like the first copy.

The simulation results show the radiation pattern of the active antenna; since antennas are reciprocal, the same pattern applies to the received signals [10] (see section 2.1). The simulations were performed in free space. The parameters frequency, spacing and rotation were varied, which will be discussed in the following sections.

[i] model available on the RNO-G GitHub page in the LPDA_analysis repository

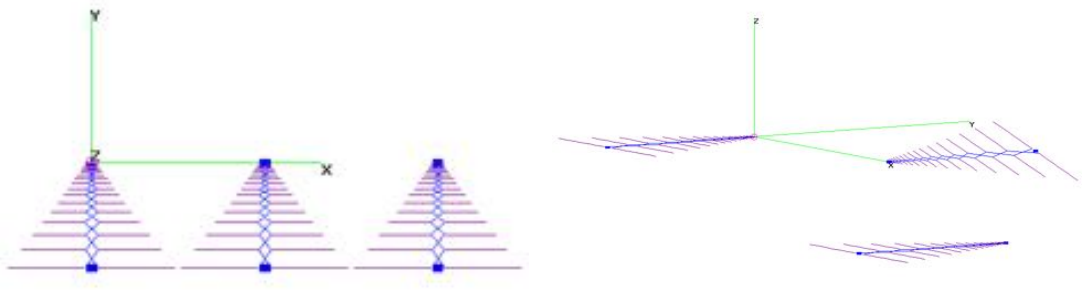

Figure 4.6: *Configurations of the three antennas modelled in the simulation. On the left side the three antennas are oriented in the same direction being* 1.5 m *apart, the z-axis is pointing upward. On the right side the spacing between the antennas is* 2 m*. Here the second antenna is rotated* 180° *in x-direction and* 30° *in y-direction, the third antenna is shifted along the z-axis.*

4.4.1 Frequency dependency

For the frequency dependence a spacing of 2 m between the antennas was used and all three antennas were pointed in the same direction (similar to left side in Figure 4.6). The frequencies 100 MHz, 400 MHz, 800 MHz and 1200 MHz show different radiation patterns, see Figure 4.7. Compared to the higher frequencies the 100 MHz pattern has a larger back lobe in both the horizontal and the vertical pattern, meaning that at lower frequencies the antenna is also sensitive in backwards direction. This leads to the conclusion that with the slightly rotated configuration in RNO-G, the lower frequencies are more affected by cross talk effects than higher frequencies.

The red dots in Figure 4.7 enclose the HPBW of the radiation pattern and the grey dots the FNBW. For the horizontal pattern all FNBW are 180°, i.e. that at 90° and 270° the intensity of the received or radiated signal is almost negligible. The −3 dB drop (HPBW) for most horizontal patterns is 60°, from 330° to 30°. The exception is 100 MHz (blue) with a beamwidth of 90°, so the signal acceptance is best at this frequency. The vertical pattern has its first null point at a higher angle and therefore the FNBW is higher than for the horizontal pattern; consequently the vertical pattern has a larger major lobe. Since the radiation pattern at 100 MHz is almost isotropic, a FNBW can not be identified, and the half power points are at the rear side of the antenna. The 400 MHz (orange) radiation pattern has also a slightly higher HPBW than the two higher frequencies.

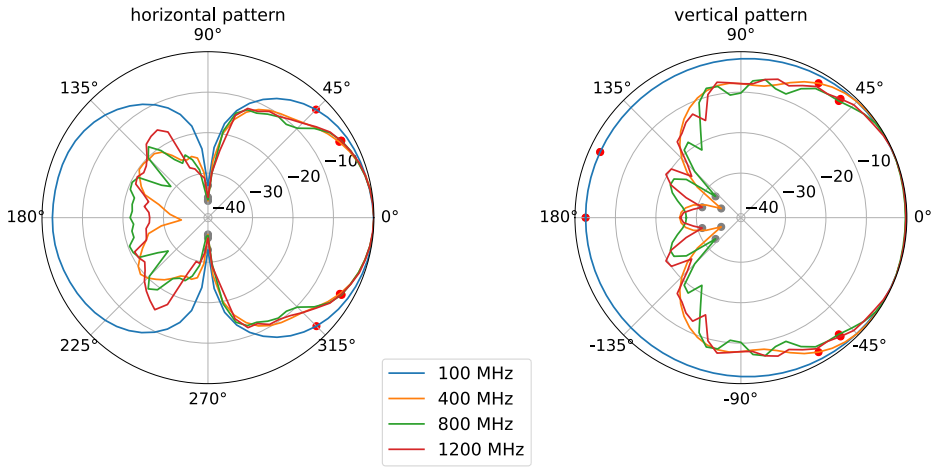

Figure 4.7: *Normalised logarithmic radiation patterns for three antennas with* 2 m *spacing at different frequencies. On the left the horizontal patterns are shown. On the right the vertical patterns are displayed. The grey dots mark the region from* 0° *to the FNBW and the red dots dots are designated to the HPBW at the respective frequency.*

A comparison with the one antenna configuration at different frequencies is possible by looking at the differences (see Figure 4.8). The differences were calculated subtracting the three-antenna simulation data from the one-antenna simulation data.

These differences can be better understood, using the theory presented in section 2.1. The importance of the major lobe has to be taken into account when looking at the differences between one and three antennas. In Figure 4.8 the FNBW regime is marked in grey and red stands for the HPBW. The unmarked differences can be neglected as those contribute to the back lobe, which is far less sensitive to a signal. In this plot the FNBW and the HPBW for the 400 MHz one-antenna case was used. Out of the four simulated frequencies, it is chosen as the most representative to give an idea about the important differences, since it is the lowest frequency of the three frequencies with similar beamwidth results.

The largest differences between the one- and three-antenna radiation patterns are found at 100 MHz for the horizontal case, both in the HPBW and the FNBW. In general, the horizontal pattern is more affected by the two passive antennas than the vertical pattern. This could be expected since the additional antennas are placed in the horizontal plane. The −3 dB-range of the vertical pattern can be claimed to be not affected, since this is a simulation and in practice these sub 0.1 dB effects are most likely lost in noise. The same might be true for the higher frequency horizontal patterns. The effects become greater when the FNBW is taken into account; here measurements are needed to determine whether or not this is a problem.

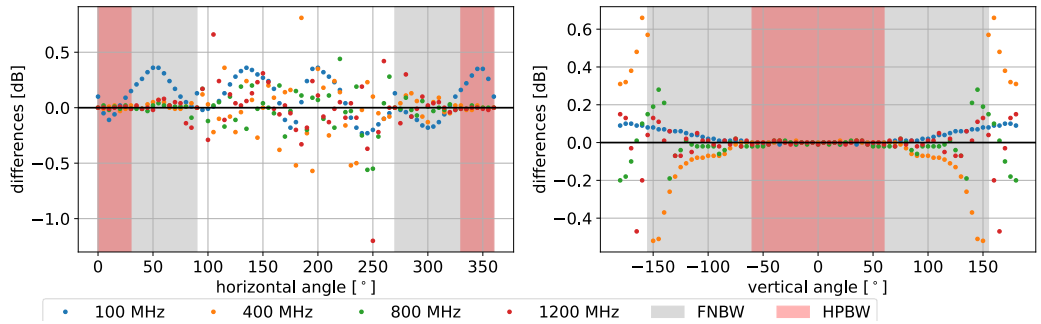

Figure 4.8: *Differences for three-antenna configuration with* 3 m *spacing at different frequencies. On the left the horizontal patterns shown. On the right the vertical patterns are displayed. The grey area marks the region of the FNBW and the red area is designated to the HPBW at* 400 MHz.

4.4.2 Spacing dependency

In Figure 4.9 the distance between the antennas was chosen to be 1.5 m (orange), 2 m (green), 3 m (red) and 4 m (purple), all antennas are pointed in the same direction. Since they are aligned in the horizontal plane, a stronger difference from the one-antenna case in this direction is to be expected.

The radiation pattern for three antennas put closest together, meaning the antennas to be 1.5 m apart (orange), show the most difference from the radiation pattern for the single antenna (blue). This can be seen in the horizontal pattern in both major lobe and back lobe as a geometric shift of the gain towards the other LPDAs. A decrease in gain in the backward direction is also visible in the vertical pattern.

For the 2 m spacing (green), which is the most interesting, only the horizontal pattern increases slightly in each direction. Therefore, the current smallest RNO-G configuration is affected by a small amount of cross talk between the antennas, but according to the simulation the three-antenna case produces a slightly higher gain than would be expected if there was just one antenna.

The average RNO-G configuration (3 m) still shows a slight difference to the one-antenna pattern. Here the gain drops compared to the one-antenna horizontal radiation pattern. The vertical pattern shows an even smaller difference.

The 4 m-configuration radiation pattern (purple) is almost invisible, because it is so close to the one-antenna radiation pattern (blue). Only relying on the eye, this means that 4 m is already sufficient to have no interaction between the antennas.

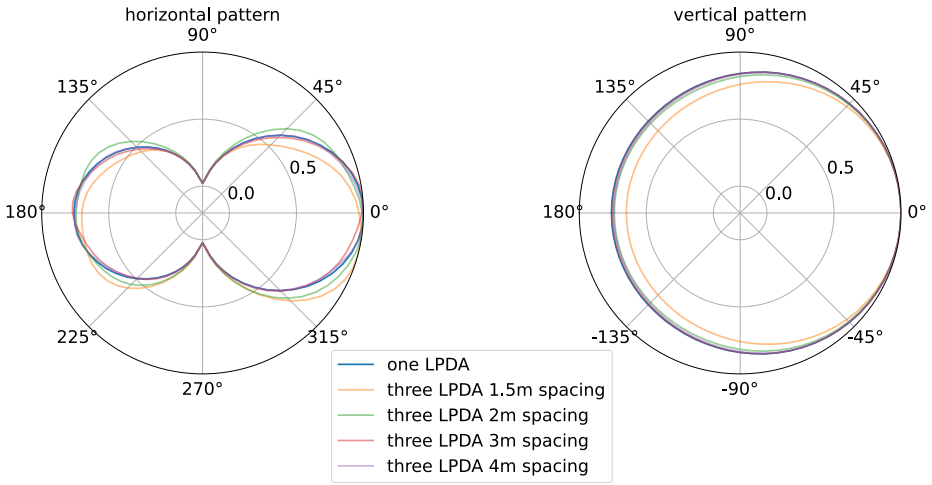

Figure 4.9: *Normalised linear radiation patterns at* 100 MHz *for different spacing of three antennas compared to one antenna in free space, with the horizontal patterns shown on the left and the vertical patterns on the right.*

This spacing relation was also simulated for 400 MHz, but no differences could be found by eye. All radiation pattern seem to be stacked on top of each other. This plot can be found in Figure C.1.

Looking at the differences of the three-antenna patterns from the one-antenna pattern (Figure C.2), even for 400 MHz a change in the pattern can be spotted. At all frequencies the differences become smaller the further apart the antennas are. This can be seen in Figure 4.10, where the range of the differences is plotted. The difference range refers to the difference between the maximal difference value and the minimal difference value in the range of the HPBW. As expected from the previous difference plot (Figure 4.8) the higher the frequency the lower the difference from the one antenna radiation pattern. The 100 MHz for 1.5 m radiation pattern is affected the most, here comes both the frequency and the spacing effect into play. This applies for the horizontal and the vertical pattern, although, as already anticipated, the vertical pattern is only affected half as much as the horizontal pattern, due to the setup.

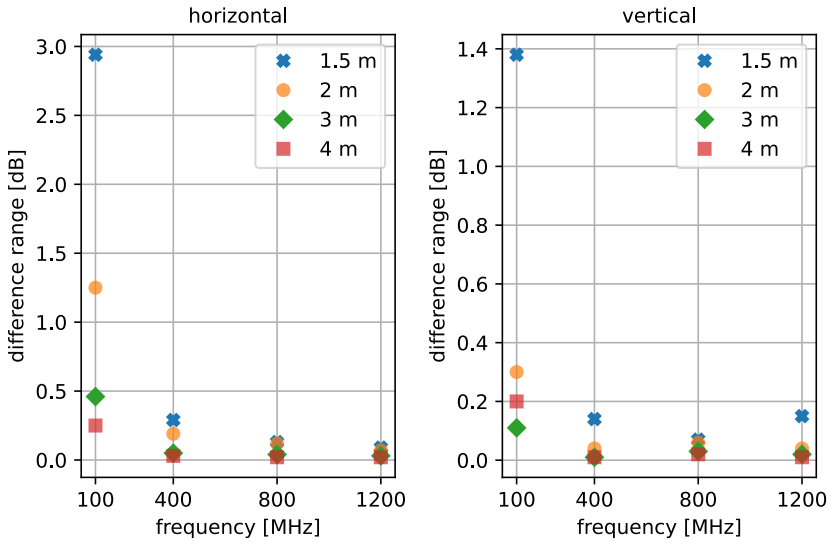

Figure 4.10: *Range of difference in the HPBW regime between one-antenna radiation pattern and three-antenna radiation pattern in* dB *over frequency for different spacing between antenna.*

In order to get an idea for the significance of the frequency and distance effect on the gain, the gain difference ratio was calculated[i]. To be more precise, the difference range in the HPBW regime was divided by the absolute value of the radiation minimum in dB for the one-antenna radiation pattern, corresponding to the signal strength. This ratio can be interpreted as the percentage the effect changes the signal amplitude. The ratios for the horizontal differences are displayed in Table 4.2 and for the vertical differences in Table 4.3. The highest difference for the horizontal pattern is 8.8 % of the signal, but especially for frequencies higher than 100 MHz the differences are lower than 1 % of the signal. The large percentages for the 100 MHz vertical patterns is a result of the isotropic high sensitivity of the radiation. It might also come into play that 100 MHz is slightly out of the LPDA's frequency regime. At higher frequencies, the vertical differences are in the order of 1 %. These results show that the simulation predicts an effect of other antennas in proximity in the order of 1 % or lower.

[i] calculation available on the RNO-G GitHub page in the LPDA_analysis repository

distance	100 MHz	400 MHz	800 MHz	1200 MHz
1.5 m	0.088	0.009	0.004	0.003
2 m	0.037	0.006	0.004	0.002
3 m	0.014	0.002	0.001	0.001
4 m	0.007	0.001	0.001	0.001

Table 4.2: *Horizontal difference ratio for the simulated radiation patterns for the different frequencies at the chosen distances.*

distance	100 MHz	400 MHz	800 MHz	1200 MHz
1.5 m	0.577	0.059	0.029	0.063
2 m	0.126	0.017	0.025	0.017
3 m	0.046	0.004	0.013	0.008
4 m	0.084	0.004	0.008	0.004

Table 4.3: *Vertical difference ratio for the simulated radiation patterns for the different frequencies at the chosen distances.*

4.4.3 Rotation dependency

In a last step different rotation angles in x- and y-direction were probed in order to provoke a change in the radiation pattern. The used rotation setups are displayed in Figure 4.6 and in Figure 4.11. The simulated radiation patterns in Figure 4.12 display next to the normally ordered 2 m spacing (see variation on the left side in Figure 4.6), a data set where the middle antenna is rotated by 180° in the x-plane (see left side in Figure 4.11), called "$x_{rot} = 180°$". Another data set, "$x_{rot} = 120°$" depicted in Figure 4.11 on the right, has both copied antennas rotated by 120° in x-direction compared to the antenna before. The last radiation pattern combines a shift of the middle antenna by 180° and a 30° rotation around the y-axis of both copied antennas (see right side in Figure 4.6). The intention behind these configurations was to turn one antenna to face the others to get most probably, the largest effect on the radiation pattern.

Even with the rotations the vertical pattern seems not to be influenced as much as the horizontal pattern. However, looking at the differences (see Figure 4.13) the vertical differences have broken their symmetry in the HPBW regime. Letting one antenna face the other two ($x_{rot} = 180°$) decreases the gain instead of increase.

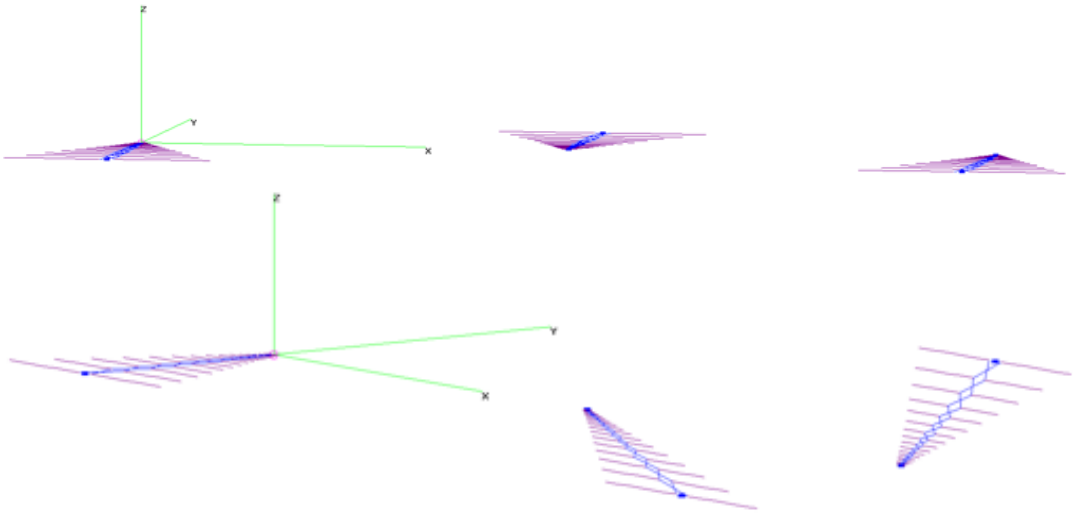

Figure 4.11: *Simulation generated picture of configurations of the three antennas placed* 2 m *apart modelled in the simulation. In the upper picture the three antennas are rotated by* 180° *in x-direction. In the lower picture the second and third antenna is rotated by* 120° *in x-direction.*

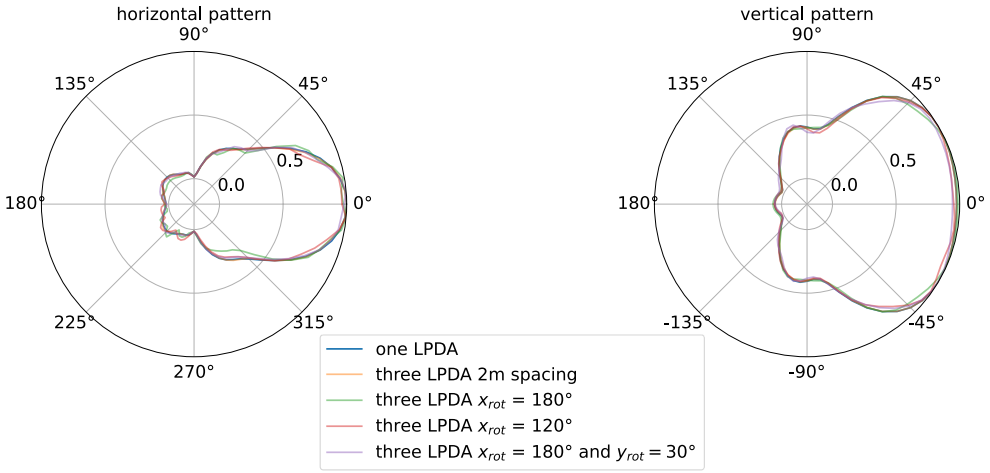

Figure 4.12: *Normalised linear radiation patterns for three antennas at* 400 MHz *with* 2 m *spacing and different rotation angles compared to one antenna in free space, with the horizontal patterns shown on the left ans the vertical patterns on the right.*

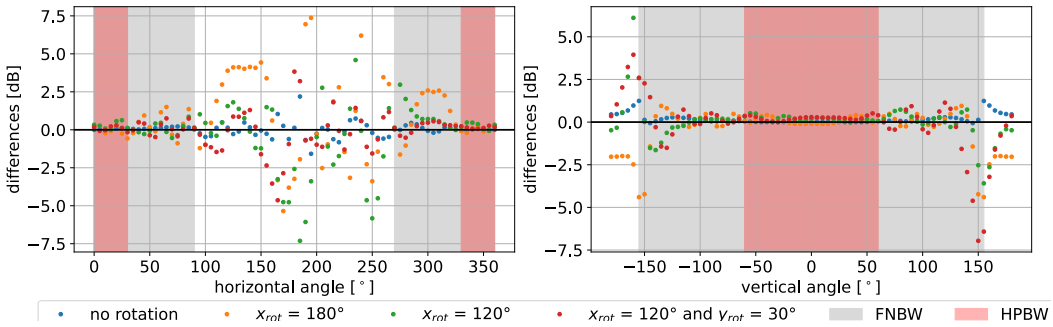

Figure 4.13: *Differences for three antennas at* 400 MHz *with* 2 m *spacing and different rotation angles, the horizontal patterns shown on the left and the vertical patterns on the right. The grey area marks the region of the FNBW and the red area is designated to the HPBW at* 400 MHz.

4.5 NEC2 simulation results

The comparison of the produced model and the instruction manual showed that the model describes the LPDA reasonably well. The voltage standing wave ratio is within the same range as specified by the manufacturer. The calculated HPBW agrees with the value given in the specifications and the overall shape of the radiation pattern looks like expected. The model is also confirmed by the calculated antenna parameters (τ and σ). Therefore, it can be assumed that the model behaves qualitatively like the actual antenna.

The simulation results show the actual presences of an effect caused by the passive antennas on the active antenna. This leads to the conclusion that in the case of RNO-G, the antenna which is surrounded by others receives a different signal than one that is not. Analysing the differences, a frequency and spacing dependency could be found. The changes in the pattern become smaller the higher the frequency is and the further apart the antennas are placed from each other. These effects on the signal amplitude are in the order of 1 % for the vertical patterns and even smaller for the horizontal patterns. An exception to this rule is the 100 MHz case, which is slightly out of the frequency boundaries of the LPDA.

In principle, the used setup for the simulation can be used for actual experiments. The difference is that a fourth antenna should be used in order to represent the neutrino source more accurately than in the simulation. The active antenna from the simulation should be used as read out antenna for the actual measurements.

5 Radio chamber measurements

To get an idea on how to achieve non-reflected signals from one antenna to another antenna, first measurements were done in the radio frequency chamber (RF chamber) of the ECAP laboratory. For this purpose sine bursts and Gauss pulse burst signals were used. Unfortunately, the chamber is too small to obtain non-reflected results, but provided a great benefit for signal study purposes. Therefore these measurements are only qualitative observations.

At the time of the cable transmission measurements (see section 5.2), the radio chamber was not yet fully functional. This affected how some measurements were done as will be discussed. There was no electricity inside the chamber and shielding was missing in the area of the door. However the electricity issue was solved for the transmission measurements from the biconical antenna to the Vpol antenna (see section 5.3).

5.1 Radio chamber setup

For these measurements a biconical antenna (BicoLOG 30100 from AARONIA AG) was used as a radiating antenna. Its frequency ranges from 30 MHz to 1000 MHz and its nominal impedance is 50 Ω [22]. Sine and Gauss bursts produced by a function generator (SIGLENT SDG6052X) were sent from the biconical antenna to a fat dipole antenna, also known as Vpol, which are used for RNO-G (see subsection 3.3.1). The Vpol is most sensitive from 150 MHz to about 600 MHz. A picture of the antennas can be seen on the right in Figure 5.1. These antennas were chosen, because they better fit the size of the radio chamber (2.5 m × 3.5 m). In these measurements frequencies from 100 MHz to 500 MHz were used, which corresponds to wavelengths of 3 m to 0.6 m. Ideally reflections should be kept at a low level, but this is not possible for the 100 MHz measurements, since one wavelength is longer than the chamber.

The radio frequency (RF) chamber is a aluminum box covered with a specific fleece to prevent noise. The fleece LBVM 1-S2 should shield the chamber against 99.999 999 % of the electromagnetic waves at 400 MHz coming from the outside [23]. It should not reflect at all, since the fleece is coated with copper, which should absorb the emitted radiation [24]. According to the manufacturer all metal objects, e.g. screws, are connected to the fleece and therefore to mass, hence they do not function as antennas.

Figure 5.1: *Photograph of the radio chamber setup. On the left: instruments outside the chamber (from left to right: voltage source for amplifier, amplifier behind oscilloscope and function generator). On the right: inside of the chamber with the biconical antenna on the left and the Vpol on the right.*

For read-out purposes the MSO54 oscilloscope with 2 GHz bandwidth and 6.25 GS/s sampling rate from Tektronix was used. The oscilloscope impedance was set to 50 Ω throughout the measurements to avoid impedance mismatch and therefore reflections of the signal. For the measurements three of the four channels were used to display the input signal of the function generator, the received signal from the Vpol antenna and the signal of the trigger. Each stored waveform contains the average over 100 triggered burst events, in order to gain more statistics and have a less noisy signal.

All the parts described above were assembled in the setup shown in Figure 5.2. The antennas were placed on opposite sides in the radio chamber, at least 50(5) cm away from the walls, most of the time at a distance of 1.00(5) m. The Vpol antenna (depicted as orange circle) was battery operated and connected to an electricity to light converter inside the chamber. For the transmission measurements a voltage supply could be used, since the chamber was fully operational by then. The signal gets transmitted via optical fibre (orange line) and transformed to an electrical signal again at the amplifier system used by RNO-G, which is fed by another power supply. The amplifier acts as a bandpass filter amplifying frequencies from about 100 MHz to 500 MHz [13]. After these steps, the signal was read out by the oscilloscope. The biconical antenna (blue circle) receives its signal directly form the function generator and is also read out by the oscilloscope (depicted by blue lines).

For the transmission measurement the function generator signal was triggered internally, depicted by the green line in Figure 5.3. This assures to trigger the wanted signal and no background events. The function generator signal occurred after a 50 ns pulse. Since the oscilloscope uses the trigger as origin for its time axis the function generator signal is displayed at 50 ns in the waveform. For the cable transmission study, the signal was triggered externally and with a trigger delay of 1.35 µs.

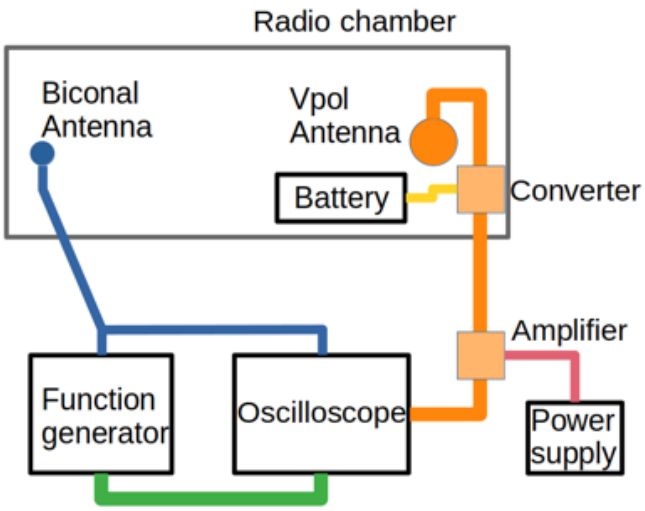

Figure 5.2: *Schematic of the radio chamber setup. Inside the radio chamber the biconical antenna (blue circle) faces the Vpol antenna (orange circle). Both are connected to their voltage sources (function generator for biconical antenna and battery for Vpol antenna) and the oscilloscope on the outside. Additionally the the Vpol antenna is connected to the converter and the amplifier. For the external trigger the oscilloscope and the function generator are connected, depicted by the green line.*

The raw oscilloscope output is visualised in Figure 5.3. Data taking starts when a trigger occurs, because of the trigger delay the signal of the function generator gets transmitted after 50 ns to the biconical antenna. This signal has a large peak and two almost vanishing peaks because of the impedance mismatch between antenna and function generator, which is discussed in section 5.2. The signal at the Vpol antenna arrives even later and no longer resembles a Gauss peak. This might be due to reflections in the cable of the emitting antenna and reflections from the chamber walls. For this reason the cable transmission was checked and some setup changes inside the chamber were made, trying to test which hypothesis is correct.

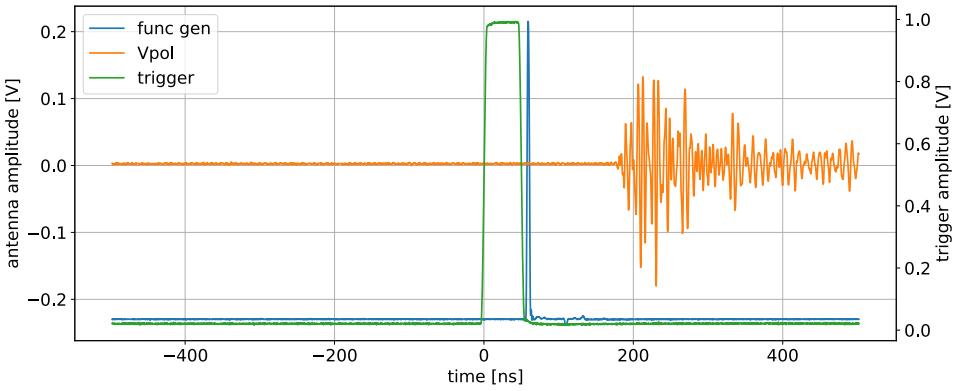

Figure 5.3: *Raw oscilloscope data from the radio chamber setup. Here a pulse burst was used to transmit a signal generated by the function generator (blue) from the biconical antenna to the Vpol antenna (orange). The data taking started with the internal trigger (green) being active.*

5.2 Cable and biconical antenna transmission study

For the cable transmission study only a part of the setup shown in Figure 5.2 was used. The function generator, the oscilloscope and the biconical antenna were needed, in order to get information about coaxial cable reflections and the frequency dependence of these reflections.

The effect of the impedance mismatch and therefore the reflection of the function generator signal in the coaxial cable was probed. A single sine oscillation burst at 100 MHz was sent from the function generator to the oscilloscope and along the coaxial cable. Three different measurements were made for a long (15.60(5) m) and a short (5.00(5) m) cable between oscilloscope and biconical antenna. The uncertainties on the cable lengths stem from measuring errors, since these lengths were measured with a folding rule and the connectors are not included.

The impedance mismatch was further investigated by terminating the coaxial cable from the function generator to the radio chamber with a resistance of 50 Ω (see Figure 5.4 on the left). In the plot the blue (long cable) and the orange (short cable) data set fuse together into a brownish colour, since both signals occur at the same time in the waveform. No reflection could be found and therefore it is confirmed that the coaxial cable has a resistance of 50 Ω as expected. In addition, it can be seen that the readout of the signal on the oscilloscope with its resistance of 50 Ω should not impact the signal or produce reflections.

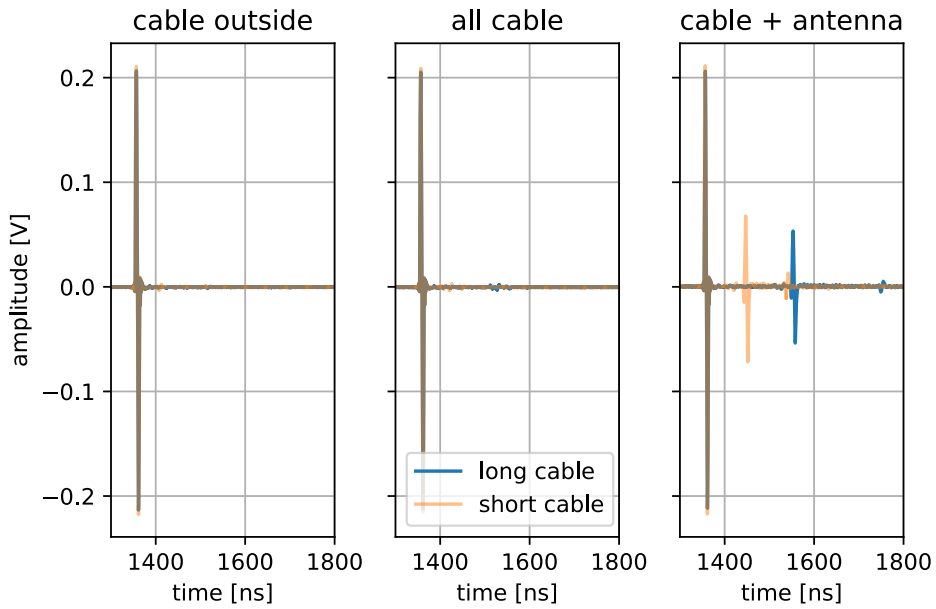

Figure 5.4: *Short (orange) and long (blue) cable comparison for different configurations. On the left only the signal transmitted by the cable outside of the chamber terminated with a 50 Ω resistance is seen. The measurement in the middle is done with all the cable inside the chamber and outside. On the right, the measurement was repeated with the antenna as terminating resistance.*

The second measurement was done using all the utilised cables for the final experiment. So the measurement contains the cable from the function generator to the chamber and the one leading into the chamber directly connected to the antenna (additional length of 3.95(5) m), but in this case to a 50 Ω termination resistance. The hypothesis was that the connection between those two cables could cause reflections, but as can be seen in the middle plot of Figure 5.4 these reflections are negligible.

Reflections arise when, instead of using the termination resistance, the biconical antenna is connected at the end (see Figure 5.4 on the right). An enhanced version of this result can be seen in the frequency dependency plot for the shorter cable (see Table 5.1). Two reflections can be seen, the first is positive and the second is negative. This leads to the assumption that the antenna impedance is higher than the 50 Ω claimed by the manufacturer [22]. In comparison to the previous measurements also a difference between the long and the short cable is now visible. In the shorter cable the reflected signal only needs 90 ns to arise after the non-reflected signal. For the longer cable the reflected signal also needs longer to be sent, it takes 196 ns to occur after the

first signal[i]. For the purposes of the wanted measurements this is appreciated, since there is more time for the pure signal to be transferred without interference of reflected signals. This effect was considered to be small, so the smaller cable was chosen out of convenience for further measurements.

One possible solution resolving the antenna impedance reflections as much as possible is to use higher frequencies. The reason is that antennas reflect differently at different frequencies as is shown by the VSWR parameter which depends on the reflection coefficient Γ (see section 2.2). It also helps with the reflection issue caused by the chamber walls, since higher frequency result in smaller wavelengths and therefore fewer reflection. For the frequency-dependence the short cable and the cables with the biconical antenna as termination was used. The results are shown in Figure 5.5.

The left-hand side of Figure 5.5 shows the full signal and how the second reflection almost disappears at higher frequencies. In this measurement the non-reflected signal is called peak 1, the voltage values for the different frequencies are displayed in Table D.1. The reflection coefficient can be calculated, using Equation 2.4 and the peak height value of the non-reflected signal (peak 1) and the first reflected signal (peak 2). Reading Table 5.1 the reflection coefficient decreases from 0.32 for 100 MHz to 0.14 for 400 MHz. Additionally, the calculated antenna input impedance can be found in the same table. The antenna input impedance was calculated rearranging Equation 2.4 to :

$$Z_{\text{in}} = \frac{\Gamma + 1}{1 - \Gamma} Z_0, \tag{5.1}$$

where Γ is the calculated reflection coefficient and Z_0 is the cable impedance of 50 Ω. From these results it can be seen that especially for future measurements frequencies around 400 MHz should be used, since here the antenna impedance is closest to the cable impedance.

frequency [MHz]	Γ	$\lvert Z_{\text{in}} \rvert$ [Ω]
100	0.32	97.1
200	0.29	90.3
300	0.22	77.9
400	0.14	66.8
500	0.17	70.4

Table 5.1: *Reflection coefficient Γ and antenna input impedance Z_{in} for cable reflection measurements for different frequencies.*

In the zoomed in version on the right side of Figure 5.5 a function generator problem starts to be visible. Without changing the amplitude settings, for higher frequencies

[i] calculation available on the RNO-G GitHub page in the LPDA_analysis repository

the output of the function generator for a single sine oscillation decreases in amplitude. This results in a signal which no longer resembles the expected sine wave structure. In general it is not advisable to use only one cycle, since it creates these small wave artefacts before and after the burst, because of the the sharp edges before and after the burst in the voltage output.

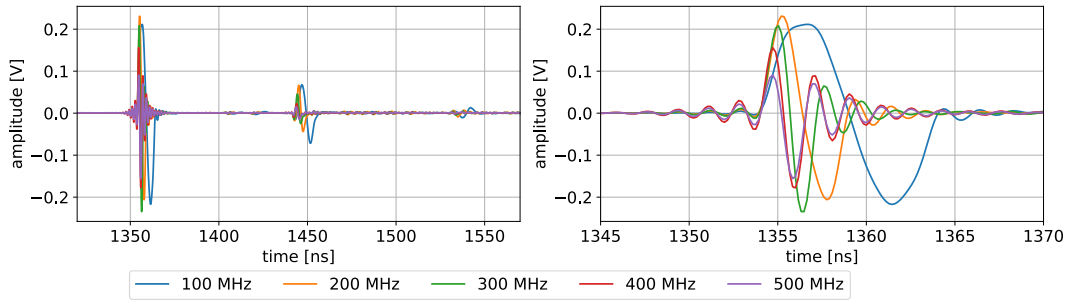

Figure 5.5: *Frequency dependence of the input signal reflection. On the left the full signal is shown and on the right it is zoomed in at the first peak.*

5.3 Transmission from biconical antenna to Vpol antenna

The transmitted signal shows, in addition to the antenna impedance reflection, a lot of reflection induced by the chamber walls (see orange waveform in Figure 5.3). This was unexpected, since the manufacturer proclaims no reflection in the data sheet of the material used to coat the inside of the chamber [23]. In order to get a better understanding where these reflections come from, two kinds of measurements were done. In the first approach the distance of the biconical antenna for two different waveforms was varied (see subsection 5.3.2), while in the second approach the number of input oscillations of the sine wave was changed (see subsection 5.3.3). Before looking at the measurements, theoretical calculations for the possible chamber reflections were performed (see subsection 5.3.1).

5.3.1 Reflection calculation

There are several possible ways for the radio wave to be reflected in the chamber. Three reflection paths of first order and the direct transmission can be seen in Figure 5.6. All paths start at the biconical antenna (blue circle in the sketch), which acts as the emitter. After the emission the radiation travels either directly (path 1) to the receiver, the Vpol antenna (orange circle in the sketch), or it reflects on the side (path 2), back (path 3) or front (path 4) wall. These paths were chosen in order to investigate

specifically the wall reflections. The path with the fastest reflected signal is of special importance since this is where the signal starts to get distorted. In contrast to the wall reflections, reflections of the ground and ceiling are negligible, when considering the vertical radiation pattern of the Vpol antenna (see Figure 3.5).

Knowing the distances between walls and antennas all wave travel distances s could be measured and with

$$t = \frac{s}{c}, \tag{5.2}$$

the travel times t can be calculated using the speed of light c as velocity.

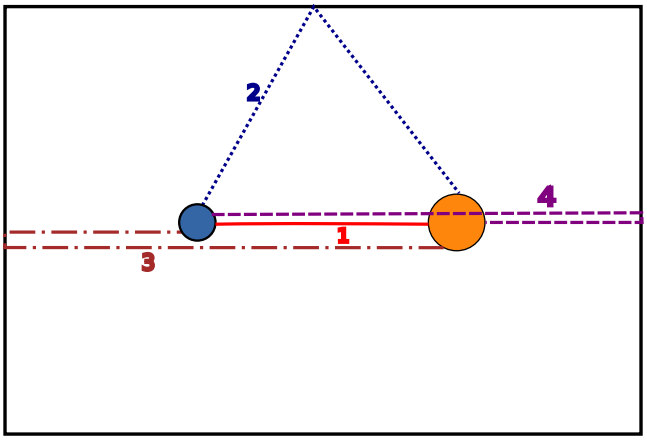

Figure 5.6: *Sketch of reflection paths (lines 2-4) in the radio chamber. Line 1 shows the direct path. The shape of the chamber floor is denoted by the black frame. The blue circle represents the biconical antenna which is the starting point of the emission and the orange circle the Vpol antenna as the receiver.*

The measured path lengths and calculated times can be found in Table 5.2. The uncertainties for the cable lengths were chosen to be ±5 cm since they were measured by hand and no connectors were taken into account. The times were used to reconstruct points in the waveform, where reflected signals could be expected. Note that the transmission time through the cable (5.06 ns/m [25]) must be taken into account as a constant offset. The cable delay was calculated to be 100.6(5) ns[i]. Another offset is the 50 ns pulse used as a trigger. The measured time from trigger to the actual signal in the Vpol antenna was measured to be approximately 183 ns for the sine measurements and 175 ns for the pulse measurement. The two calculated offsets of the cable delay and delay caused by the trigger do not add up to the measured signal delay. The difference between the calculated and actual time delay was assumed to be caused by a

[i] calculation available on the RNO-G GitHub page in the LPDA_analysis repository

delay in amplifier and converter. The results for path 1 are displayed in Figure 5.7 and Figure 5.8 as a red line, called "start". The other paths were also used in Figure 5.8.

path	s [m]	s [λ]	t [ns]
1	1.19(5)	1.19(5)	3.97(17)
2	2.52(5)	2.52(5)	8.40(17)
3	3.19(5)	3.19(5)	10.64(17)
4	3.41(5)	3.41(5)	11.37(17)

Table 5.2: *Path lengths s in meter and wavelength λ for 300 MHz ($\lambda = 0.999\,\mathrm{m}$) and calculated times t (Equation 5.2) for a distance of 1 m between biconical antenna and the nearest wall.*

5.3.2 Waveform and distance variation

As mentioned in section 5.3, the first approach, varying waveform and distance, was used to optimise the used waveform for the burst. A burst, i.e. a short signal, was used to better track interference that could go unnoticed in a continuous signal, due to matching periodicity. Looking at the simulated electric field response in Figure 3.2, a single sine oscillation signal would be a good choice, in order to create an artificial neutrino signal. When using this type of waveform in the previous measurement, the signal amplitude problem and the artefact problem occurred. Hence another solution was needed. A pulse waveform would have less artefacts before and after the signal and therefore have closer resemblance to a distinct one peak signal. Another possibility is to use a sine signal with the length of few full oscillations, in this case three, in order to reduce the artefact and signal amplitude problem.

At the same time the emitter-receiver distance was varied for the two waveforms. To achieve this position difference the Vpol antenna (receiver) stayed fixed and the biconical antenna (emitter) was moved. The back wall (wall on the right in Figure 5.6) of the radio chamber was used as a reference point. The measurements were carried out by placing the biconical antenna 0.5 m, 1 m and 1.5 m away from the back wall. Therefore the distances between the two antennas are 1.69 m, 1.19 m and 0.69 m, respectively. All these distances have an estimated uncertainty of ± 5 cm; for clearer visibility the display of the uncertainty will be renounced in the future.

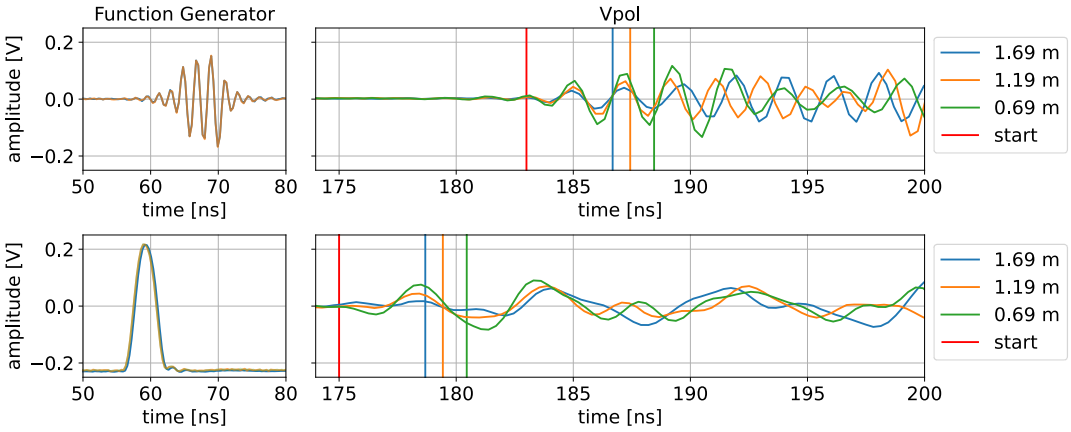

Figure 5.7: *Three-sine burst measurement (upper row) and pulse burst measurements (lower row) at different distances between emitter and receiver: on the left column is the generated signal sent to the transmitting biconical antenna. On the right column is the received signal from the Vpol with estimated time of reflection signal arrival for path* 2*. The vertical lines represent the calculated time of arrival of the path* 1 *signal in red and the path* 2 *signal in the corresponding distance colours.*

The biconical antenna signal for the pulse starts roughly 8 ns earlier than the sine burst, which leads to the same signal shift in the Vpol antenna. The sine burst generated by the function generator has an amplitude of 320 mV and a frequency of 300 MHz. The highest frequency that can be achieved with the pulse burst is 150 MHz. This is a disadvantage, since it has been shown that the frequency required for less reflection is 400 MHz. The function generator signals are seen in the left column of Figure 5.7.

The signals received by the Vpol antenna are shown in the right column of Figure 5.7. All Vpol signals were shifted by the amount of time needed to get a non-reflected signal between sending and emitting antenna[i]. This procedure aligns the signals to start at the same time, resulting in a better comparison. The red vertical line marks the start of the signal transmission. The other coloured vertical lines show where the reflected signal with the shortest distance (path 2) occurs for the different distances between the antennas. The colours correspond to the waveforms with the same colour. For example the blue waveform shows the waveform for the largest distance (1.69 m) between the antennas. Looking at the range of the signal between the start point, marked by a red line, and the blue line, the signal seems to behave as expected. After the blue line, when the fastest reflected signal hits the antenna and the direct and the reflected signal interfere, the recorded waveform deviates from the shape it had before. This is especially visible in the case of the pulse burst. A slight deviation

[i] calculation available on the RNO-G GitHub page in the LPDA_analysis repository

from the function generator signal is expected, due to the antenna response. The antenna response should not influence the frequency, i.e. distance between null points, of the signal. Therefore the variation in amplitude and width of the pulses can not be fully explained by the antenna response. These longer high level periods indicate a superposition of multiple signals with different phase and therefore lead to interference of the reflected signals. With the sine burst, this effect is way more difficult to see, because the signal is longer and has more peaks, but a slight change in peak width is visible.

5.3.3 Variation of number of sine oscillations

In Figure 5.8 different numbers of oscillations of a sine wave were used in order to provide better understanding of the chamber reflections already suspected in Figure 5.7. Without probing different distances the chamber wall reflections are also visible using the sine burst signal. The times from Table 5.2 are shown by vertical lines in this plot. For the direct signal that starts with the red vertical line, all waveforms have the same shape, but after the signal from the second path starts, the signals for the three different waveforms change in different ways. When path 3 and path 4 hit, the interference of the signal is clearly visible, especially for the one-sine oscillation waveform (blue). Another strong indication for interference in this plot is the repeating wave package structure, since a single distinct burst would be expected if no interference occurs. With three-sine oscillations the burst is still visible in the interference patterns, compared to the one-sine oscillation.

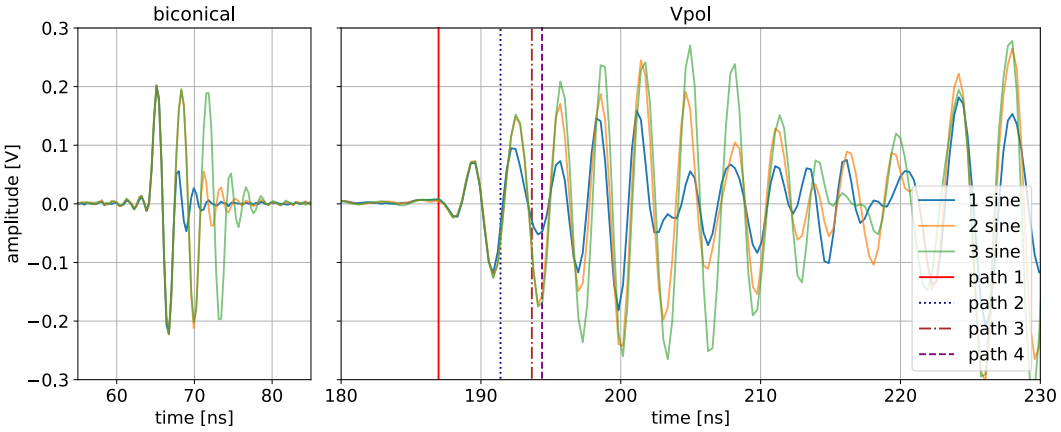

Figure 5.8: *Burst measurements with different number sines. On the left the generated signals with one, two and three sine oscillations starting at* 64 ns *sent to the transmitting biconical antenna. On the right the received signal from the Vpol with estimated time of reflection signal arrival as vertical lines.*

In addition, the antenna linearity can be demonstrated with these measurements. This was done by subtracting the one oscillation sine wave pattern from the two oscillation sine wave waveform and the two oscillation sine wave from the three oscillation sine wave data set[i]. If linearity is fulfilled all waveforms should be the same since they should only contain the response to one-sine wave after the subtraction. This was done in Figure 5.9.

Since all signals start at the same time (186.87 ns) the first oscillations get removed, meaning the subtraction shifts the signal one (3.3 ns at 300 MHz) and two sines (6.6 ns at 300 MHz) respectively in time. This offset was removed to see the waveforms stacked on top of each other.

With the subtraction all three measurements have the same pattern, except for the range from 219 ns to 236 ns (black vertical lines). Since these changes are only in amplitude and not in frequency it is believed that they stem from digitisation errors and do not falsify the claim of linearity.

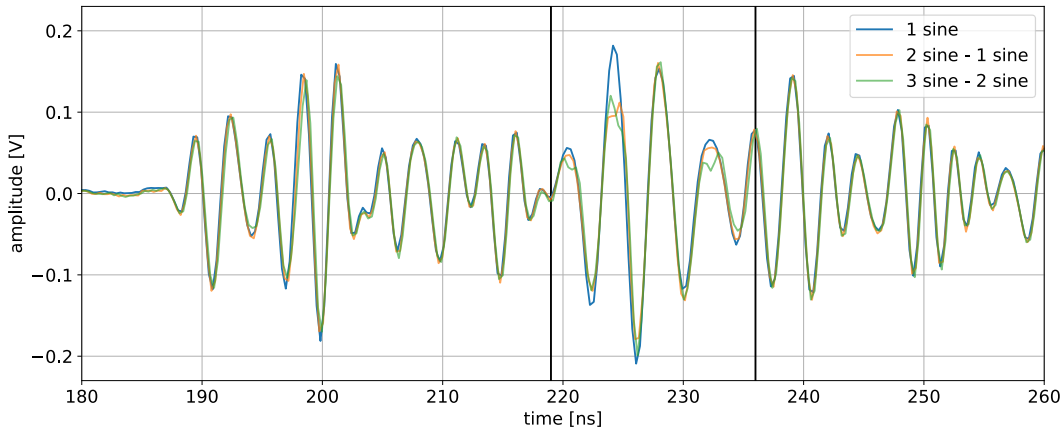

Figure 5.9: *Burst measurements with different number sines subtracted to only show one-sine wave. The "2 sine - 1 sine"-measurement is shifted by −3.3 ns and the "3 sine - 2 sine" measurement is shifted by −6.6 ns. Stronger variations occur between the two black vertical lines.*

[i] calculations available on the RNO-G GitHub page in the LPDA_analysis repository

5.4 Radio chamber measurement results

The measurements in the radio frequency chamber showed that the antenna is not terminated with an impedance of 50 Ω. Therefore a small antenna impedance reflection signal is to be expected. Since the cables are long enough, the reflected signal occurs long after the actual signal. Therefore the reflected signal originating from the impedance mismatch does not overlap with the non-reflected signal.

The other result obtained from these measurements is that the chamber is not suitable for measurements with two antennas inside, due to extreme chamber reflections. More space is needed in order to see only the influence of other antennas and no walls, desks etc. For this reason the experimental hall of the ECAP laboratory was chosen for the performance of further measurements.

Investigating different waveforms showed that a three oscillation sine burst should be a good choice for further measurements. The wave package is still visible in interference patterns. A balance between correct signal display of the function generator (smaller frequencies desirable) and a reasonable frequency to prevent antenna impedance reflections (better with higher frequencies) must be found. Therefore future measurements will be conducted at 400 MHz in order to be in the cable reflection minimum.

Using the converter and amplifier system of RNO-G is useful to see the signal that is generated by stations and worked with, but they also change the signal slightly. In order to have the pure antenna response these components should not be added in future measurements.

6 Experimental hall measurements

After finding an effect on the emission characteristics on an antenna when other antennas are placed in close proximity to that antenna in simulations (see chapter 4), these results need to be verified. Since only two antennas fit into the RF chamber and several other problems occurring during the measurements there (see chapter 5), the experimental hall at ECAP laboratory was chosen to host the next set of experiments. Due to the vast size of the hall, it was possible to fit four antennas in appropriate distances to each other into the hall without getting reflections from the walls.

6.1 Experimental hall setup

These measurements try to mimic the setup of the surface antennas of RNO-G as well as possible. Therefore, three LPDAs are placed on tripods at the same height next to each other 2 m or 3 m apart, as they would be in the ice. The two outer antennas are rotated by 120° outwards. This can be seen in the upper inset in Figure 3.3. The middle one faces the biconical antenna, which imitates a neutrino signal source.

Learning from previous measurements and the simulations, the signal for the experimental hall measurements is optimised. According to the results from the radio chamber measurements (see section 5.4) the best waveform is a three-sine oscillation burst, in order to spot the burst in possible reflections. It is known that the frequency influences the antenna impedance (see section 5.2), hence the frequency (400 MHz) will be probed. The angle dependency at different frequencies used in the simulation are not suitable to test with measurements, due to the function generator capability of probing only up to 500 MHz and the risk of ground reflections, if the wavelength is too long.

For signal read-out purposes the same instruments are used as for the radio chamber measurements (see section 5.1). The SIGLENT SDG6052X function generator sends its signal via coaxial cable to the biconical antenna (BicoLOG) which transmits this signal to the LPDAs. The MSO54 oscilloscope with 1 GHz bandwidth and 6.25 GS/s sampling rate, reads out the function generator signal and one of the LPDA signals. In this case no amplifier or voltage sources are needed, which leads to a pure and unfiltered signal from the antenna.

For all measurements the receiving LPDA was mounted on the carbon tripod C6i from Rollei [26], which has a ball joint with a horizontal angle scale (5° steps).This allows to rotate the antenna without turning the tripod. The rotation capability was very important for the radiation pattern measurement. The antenna was mounted at the centre of gravity rather than the middle of the boom. The mounting plate is placed at the 14th element (see Figure 4.1). The distance between receiving and sending antenna varies about 50 cm over the course of the radiation pattern measurements.

The other two LPDAs were mounted on wooden tripods. Those tripods had no possibility to measure angles. Therefore, the angles needed for the RNO-G setup were measured, using a measuring tape and triangle relations.

6.2 Measurement signal and uncertainties

In order to understand the measurement results, the signal retrieved from the LPDA and the measurement uncertainties had to be studied. Both systematic uncertainties and statistical uncertainties were investigated. For these measurements only one receiving LPDA and the emitting biconical antenna were used. The setup for these measurements is shown in Figure 6.1. Both antennas face each other directly in order to get the highest signal amplitude possible.

Figure 6.1: *Picture of the setup for the distance variation in the experimental hall. biconical as the emitter (on the right) and LPDA as receiver (on the left) face each other directly.*

6.2.1 LPDA received signal

For each measurement a three-sine oscillation burst with a frequency of 400 MHz was used. The reason for choosing this signal was discussed in section 5.4. The function

generator signal which was sent to the biconical antenna can be seen in Figure 6.2. The signal emitted by the biconical antenna and received by the LPDA was captured by the oscilloscope. It was averaged by the oscilloscope over 500 triggered events. Comparing the function generator signal to the LPDA signal both contain more than three sine oscillations, but the LPDA receives the amplitudes differently than they were sent to the biconical antenna. The reason for the function generator signal containing more than three oscillations was due to the effect explained in section 5.2.

Two LPDA-received signals for the radiation pattern measurement can be seen in Figure 6.2. The "0° LPDA" measurement (orange) shows the maximal signal in the horizontal radiation pattern data set. The "180° LPDA" measurement (purple) shows one of the minimal signals in the horizontal radiation pattern data set. Looking at all data sets at once, the samples shaded in grey seem to always contain the maximal signal[i]. In case of the radiation pattern measurements the range between 4100 and 4178 samples, containing the maximal amplitude, was used in order to make sure to get the signal amplitude and not an accidentally high noise amplitude. The signal peak-to-peak voltage for the measurements was calculated from this range.

The peak-to-peak voltage V_{pp} was chosen, because of the offset of approximately $-0.2\,\mathrm{mV}$ in some measurements. The origin of this baseline difference is unknown. the peak-to-peak voltage was calculated subtracting the minimum voltage in the signal range V_{min} from the maximum voltage in the signal range V_{max} (see Equation 6.1). With this procedure the amplitude is independent of the voltage offset and an absolute value.

$$V_{\mathrm{pp}} = V_{\mathrm{max}} - V_{\mathrm{min}} \tag{6.1}$$

Often measurements will get compared with each other, therefore the difference ΔV_i of each sample i in the two data sets n and m with voltage $V(n)$ and $V(m)$ (see Equation 6.2) will be calculated. The peak-to-peak voltage will be used as a reference point in the following to calculate the deviation $\Delta V/V_{\mathrm{pp}}$.

$$\Delta V_i = V_i(n) - V_i(m) \tag{6.2}$$

A possible reason for the higher amplitude noise sequence shortly after the LPDA received signal (see Figure 6.2, measuring at 0°) could be a slight afterringing. Since this phenomenon is visible for all measurement this seems to be a systematic issue. It will not be investigated any further.

[i] script available on the RNO-G GitHub page in the LPDA_analysis repository

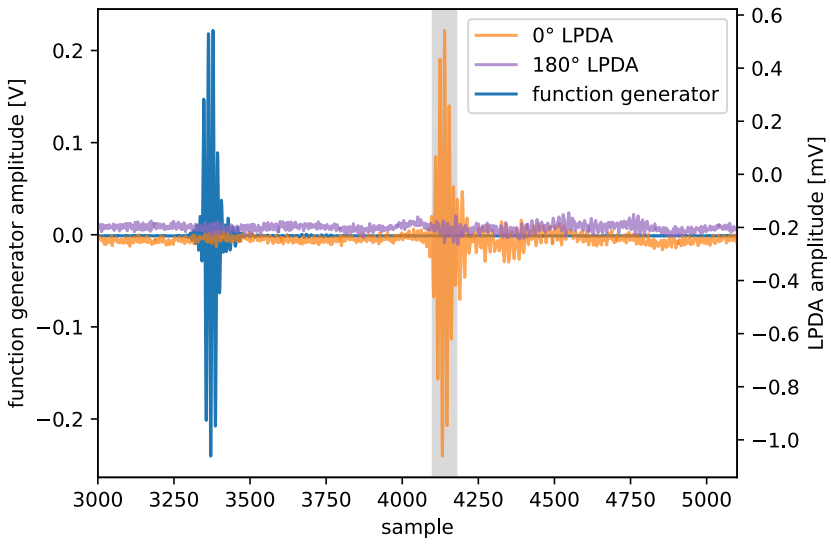

Figure 6.2: *LPDA signal directly facing the sending biconical antenna (orange) and LPDA signal facing the opposite way (purple). The amplitude axis corresponding to these data sets is shown on the right. The y axis on the left is for the function generator signal (blue). The grey window marks the signal location in the waveforms.*

6.2.2 Statistical uncertainties

The setup with one LPDA (see Figure 6.1) was used to estimate the statistical error of the signal amplitude. This is especially important for the three-antenna measurements in order to be sure how significant the deviations from the one-antenna scenario are and how much the statistical contribution is. For this purpose 350 measurements at a distance of 1.5 m from biconical antenna to LPDA, each averaged over 500 triggered events, were taken to get more statistics.

First the maximal peak-to-peak voltage was calculated and a histogram created, one bin contains three voltage steps. As can be seen in Figure 6.3, the central limit theorem can be applied and a Gauss fit can be performed on the histogram data. The mean maximal peak-to-peak voltage for this setup was calculated to be 14.976(2) mV and the standard deviation is 0.034(2) mV. For future measurements the standard deviation of 0.03 mV will be used as statistical uncertainty, since further measurements will not be conducted with such high statistics.

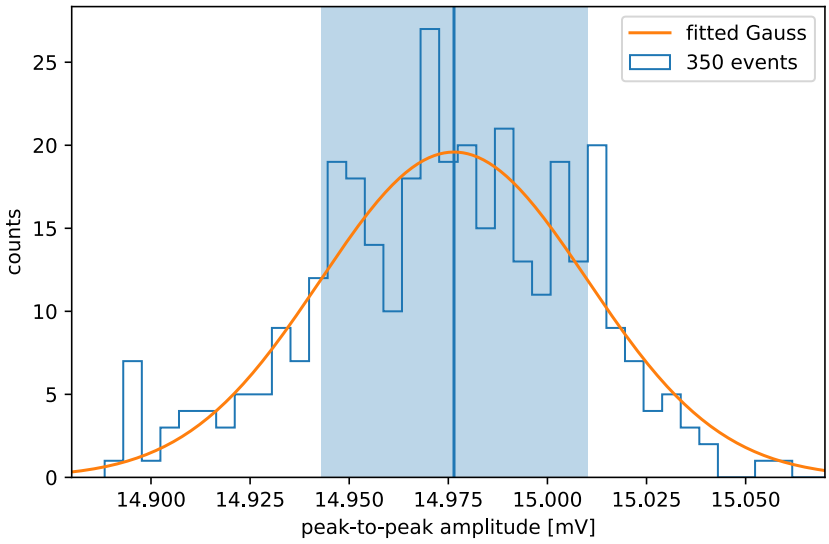

Figure 6.3: *Histogram of peak-to-peak voltage spectrum for* 350 *measurements with Gauss fit, mean (blue vertical line) and* 1σ *interval (light blue shaded area).*

6.2.3 Systematic uncertainties

Two types of systematic uncertainties were found for these measurements. The distance variation plays an important role, because of the asymmetry while rotating the LPDA (see section 6.1) and the general position inaccuracy. In addition, a time jitter, most likely induced by the oscilloscope, had to be taken into account. Both error sources could be compensated.

Distance variation of the antennas The used signal window of 78 samples is wider than the expected sample size for three sine oscillations (47 samples), because of the already mentioned distance variation between the antennas and hence the shorter or longer signal travelling time. In order to investigate this, a slight distance variation was probed. Distances were chosen corresponding to factors of the wavelength at 400 MHz. The arbitrarily chosen factors are 1.75, 2, 2.25 and 2.4. This leads to a spacing between the emitting biconical antenna and the receiving LPDA of 1.31 m, 1.5 m, 1.68 m and 1.8 m, respectively.

The setup for these measurements is shown in Figure 6.1. Both antennas face each other directly in order to get the highest possible signal amplitude. The LPDA stayed in the same position and the biconical was moved in order to vary the distance.

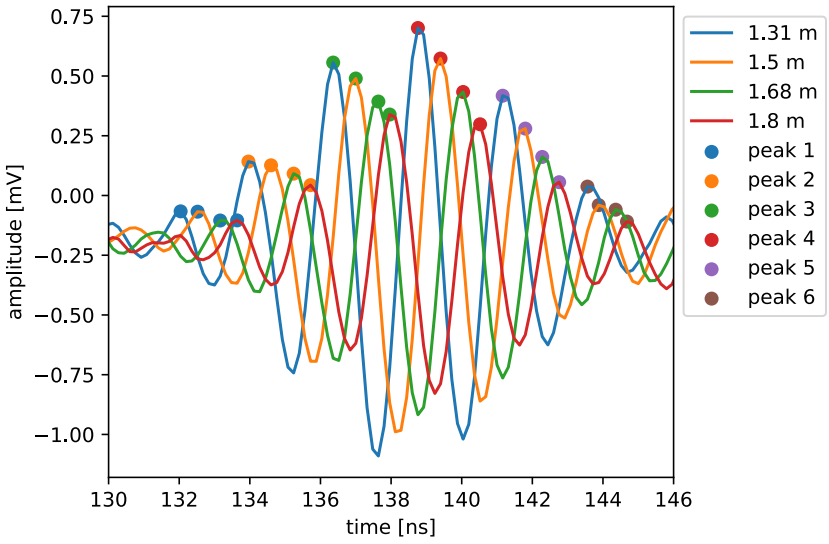

Figure 6.4: *LPDA signal for different distances between receiver and emitter. Each peak is marked with a dot, the colour corresponds to the number of peak in waveform.*

The results of the distance variation are shown in Figure 6.4. The waveforms for the LPDA signal are displayed in the time range corresponding to the discussed sample window. As already discussed in the previous sections there are more than three peaks in the waveform. The prominence option in the `find_peak` algorithm (`scipy.signal` python package) was chosen such, that in total six peaks could be identified. The waveforms are delayed in time proportional to the different distances, as can be seen in Figure 6.4.

According to the inverse-square law, the amplitude of the signal amplitude is expected to decreases with $\frac{1}{r}$ over the distances $r = 1.31\,\text{m},\ 1.5\,\text{m},\ 1.68\,\text{m}$ and $1.8\,\text{m}$. Additionally, the active region had to be considered. The active region can be determined using subsection 3.3.2 and comparing the half wavelengths with the dipole lengths in Table B.1. For the chosen frequency of $f = 400\,\text{MHz}$, which corresponds to half a wavelength of $\lambda/2 = 0.375\,\text{m}$ the active region is the dipole 9 with a length of $0.34\,\text{m}$. Therefore a constant offset of $0.266\,\text{m}$ (boom position) in addition to the feeder length of $0.04\,\text{m}$ must be taken into account.

In the representation shown in Figure 6.5 a linear fit (see Equation 6.3) was performed. The parameter a denotes the slope and the parameter b the y-axis offset. For the r values a Gaussian error propagation[i] was performed and the amplitude A uncertainty of $0.03\,\text{mV}$ from subsection 6.2.2 was used.

[i] calculation available on the RNO-G GitHub page in the LPDA_analysis repository

$$A(r) = a \cdot \frac{1}{r} + b \tag{6.3}$$

Since all the reduced χ^2-values for the fits are close to 1, the assumption that the inverse-square law applies seems true. But each peak in the waveform has a different slope (see Table 6.1). Therefore no general assumption can be made about the voltage decrease at a certain distance. Within the measurement uncertainties all data points lie on the fit, which leads to the assumption that the uncertainties are overestimated slightly.

peak	slope [mVm]	offset [mV]	$\frac{\chi^2}{\text{d.o.f.}}$
1	0.31(27)	−0.25(15)	0.16
2	0.64(27)	−0.24(15)	0.44
3	1.52(27)	−0.37(15)	0.47
4	2.71(27)	−0.96(15)	1.61
5	2.45(27)	−1.09(15)	0.48
6	0.94(27)	−0.55(15)	0.26

Table 6.1: *Fit parameter and reduced χ^2-values ($\frac{\chi^2}{\text{d.o.f.}}$) for the linear fits (see Equation 6.3) performed for the verification of the inverse-square law.*

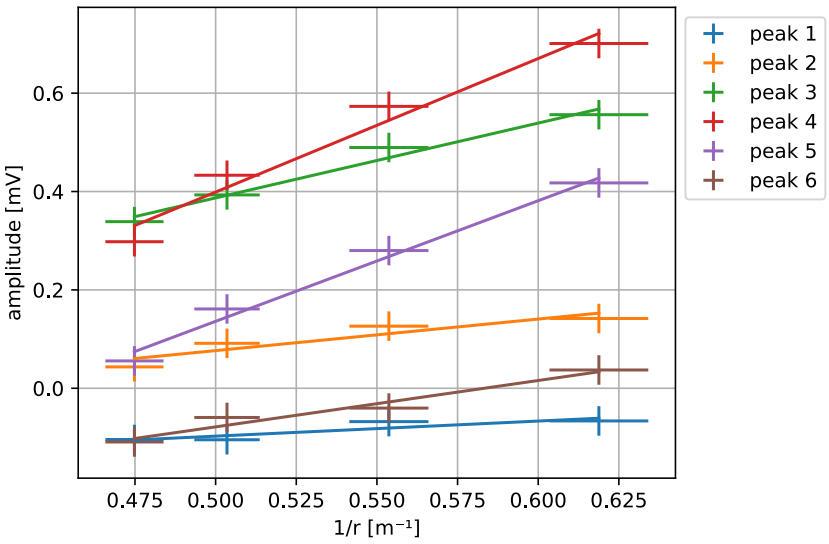

Figure 6.5: *Inverse distance over voltage for the peaks in Figure 6.4 and corresponding linear fits.*

Time jitter of the oscilloscope Comparing the signal and the associated differences, subtraction of one data set from another, shows that the differences have maxima at the zero passages of the signal (see Figure 6.6). This leads to the conclusion that the difference is caused by a shift in time. In order to prove this a cross correlation of the signals was done. With the correlation function of the `scipy.signal` python package in "full" mode the timing difference could be calculated. Is the maximum of the correlation not in the $(n-1)/2$ sample of the correlation, the signals are time shifted by the amount of samples lying between maxima sample and $(n-1)/2$ sample[i].

For a better resolution, the signal was upsampled by a factor of 100. This procedure is not without risk. Since the additional data points are effectively the result of an interpolation, it is not clear whether the newly created data points represent reality. It is believed that the original sampling is good enough to detect all the physics in the signal and the resampling only reinforces the structure of the signal. Nevertheless, sampling errors can arise from this procedure.

The comparison of the differences to the signal before and after the shift are shown in Figure 6.6. The differences get smaller after they are shifted to the same waveform starting point. There is almost no amplitude difference between first and second data set. Therefore they agree very well. This implies that the error from the time shift can be fully removed. This procedure is applied to every data set where differences are needed for the analysis in order to get only the amplitude difference and not the time jitter.

The time jitter for the first 150 data sets of the statistics data sets are shown in the histogram in Figure 6.7. To keep computing time reasonable, cross correlations were not calculated for all 350 available data sets. The maximal time jitter of $-0.0416\,\mathrm{ns}$ corresponds to 0.26 original samples. So this effect is presumed to stem from the oscilloscope.

[i] script available on the RNO-G GitHub page in the LPDA_analysis repository

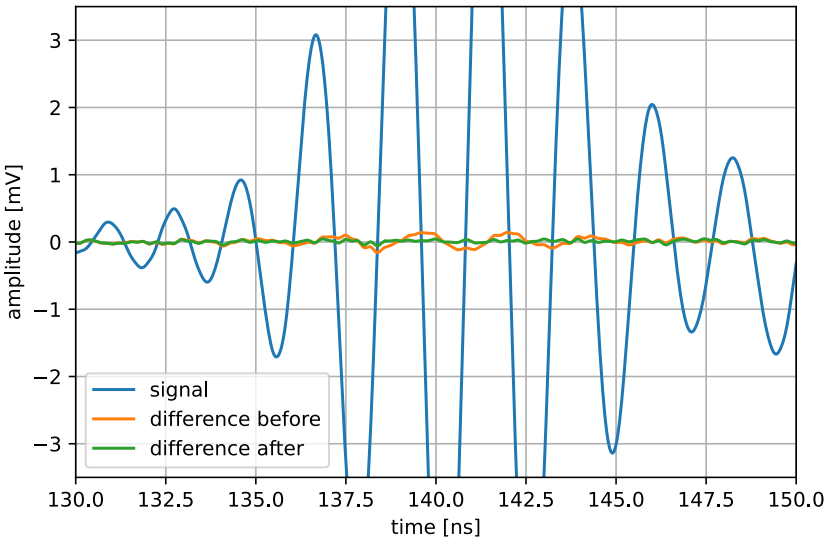

Figure 6.6: *Signal of a statistics measurement with the differences from the first statistics data set. The differences before the time shift and after the time shift are displayed. All data sets are upsampled.*

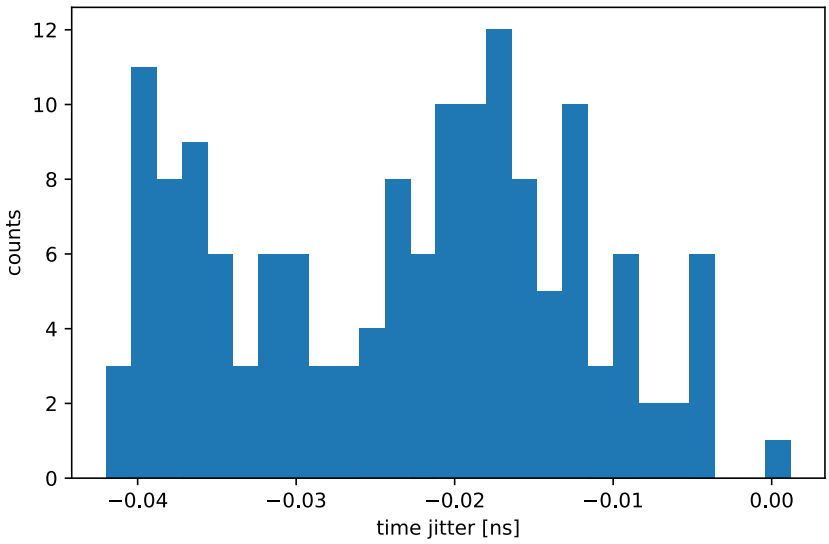

Figure 6.7: *Time jitter distribution for the first* 150 *data sets of the statistics data sets. One bin corresponds to* 0.0016 ns.

6.2.4 Sanity check

In order to check if the setup works properly, a sanity check was performed. For this measurement first the received signal of a single LPDA was measured with the same setup as in Figure 6.1. For a second measurement the other two LPDAs were placed touching the receiving LPDA. The later procedure should provoke a completely altered behaviour from the receiving antenna.

The result is shown in Figure 6.8. As predicted the signal amplitude of the touching three antennas varies a lot from the one-antenna signal. It is broader in time and has less amplitude than the expected signal. Hence, the setup seems to deliver valid results for the desired purposes.

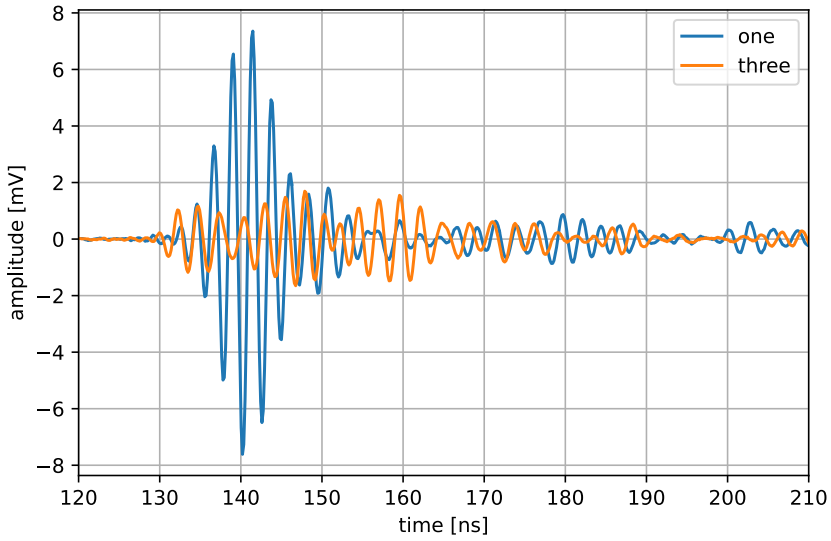

Figure 6.8: *Signal of one LPDA receiving the signal with no other antennas in the surrounding area ("one"). And the signal of one LPDA receiving the signal with two other antennas touching the signal receiving antenna ("three").*

6.3 One LPDA radiation patterns

The measurements with one LPDA were made to compare with the three-LPDA measurements, but also to measure a full radiation pattern, or to be more precise a receiving pattern (the same due to reciprocity, see section 2.1), of the LPDA and compare it with the simulation.

The normalised linear gain was measured the same way for the horizontal and the vertical pattern. The peak-to-peak voltage explained in subsection 6.2.1 was used. For the normalisation the highest amplitude of the data set was selected as normalisation factor[i]. This leads to a voltage gain between 0 and 1, which is comparable to the linear gain in the simulations.

Another question that arises is whether the distance of 1.5 m between sending and receiving antenna is sufficient to be considered as far field. This can also be probed with the simulated radiation patterns, since they are known to represent the far field pattern. If the simulated and measured pattern match, it is assumed that they both show the far field. Using the Equation 2.3 and the frequency of $f = 400\,\mathrm{MHz}$, which corresponds to a wavelength of $\lambda = c/f = 0.75\,\mathrm{m}$, and the largest antenna dimension being the longest dipole with $D = 1.45\,\mathrm{m}$ (see Table B.1) the far field radius is calculated to be:

$$r_{\text{LPDA far field}} \geq \frac{2 \cdot 1.45\,\mathrm{m}^2}{0.75\,\mathrm{m}} = 5.6\,\mathrm{m}. \tag{6.4}$$

This result leads to the conclusion that the measurements were not performed in the far field.

The simulation for comparison is performed for free space, since the conductivity of the ground was unknown. The vertical pattern should be less accurate, due to the higher effect of the ground towards the floor. Note that the simulation represents an actual radiation pattern opposed to the receiving pattern that is measured. Due to reciprocity (see section 2.1), the two patterns are the same.

Horizontal radiation pattern The horizontal pattern was measured in 15° steps rotating the LPDA anti-clockwise. The starting point (0°) is the LPDA facing the biconical antenna. One of the measurements is displayed on the left side of Figure 6.11. As can be seen on the right in Figure 6.9 the angle marks on the rotational angle scale shows 5° steps, therefore the angle uncertainty was chosen to be ±2°.

[i] calculation available on the RNO-G GitHub page in the LPDA_analysis repository

Figure 6.9: *Photographs of the setup for horizontal radiation pattern measurement for 105° on the left. The blue biconical antenna is the radiating antenna and the LPDA on the left is the receiving antenna. On the right the rotational angle scale is shown, which is used to identify the angle.*

Looking at the measured and simulated horizontal pattern in Figure 6.10 the resemblance is good. Both patterns are normalised to the radiation maximum, which corresponds to the voltage at 0°. In the case of the measurement the maximal horizontal peak-to-peak voltage is 1.60(3) mV. The normalisation factor for the simulation is unknown. The major lobe for the measured data is smaller in radius than the simulation, while the outward curvature around 60° and 290° is missing. The back lobe is a slightly bigger, but within the chosen uncertainties.

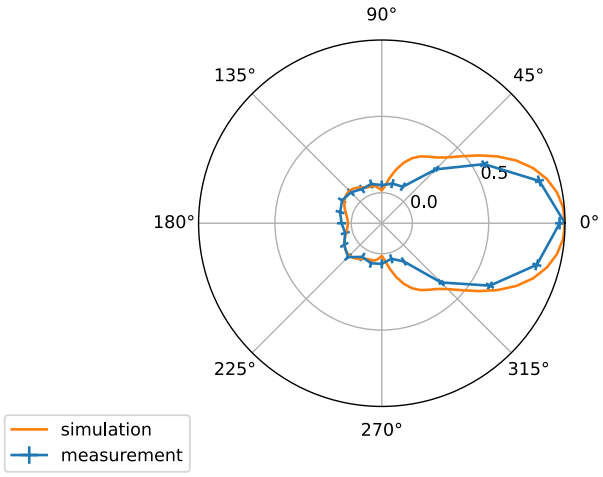

Figure 6.10: *Measured and simulated horizontal linear gain radiation pattern, normalised to the radiation maximum. Simulation shows free space pattern. Measurement contains ground.*

Vertical radiation pattern The measurement of the vertical pattern was a bit more difficult, due to the ball joints high rotational degrees of freedom. Since making adjustments in the vertical plane was not easy, the size of rotation steps was increased to 30°. The inclination was monitored using the inclination tool provided by the app Phyphox [27], which is an Open Source Software from RWTH Aachen, using smartphone sensors to accumulate data for experiments. A picture of the phones position on the antenna to measure the inclination can be seen in Figure 6.11 on the right. Here again the starting point (0°) is the LPDA facing the biconical antenna. One of the measurements is displayed on the left side of Figure 6.11. Due to the ball joint, the angle uncertainty was estimated to be ±3°.

Figure 6.11: *Photographs of the setup for vertical radiation pattern measurement for 45° on the left. The blue antenna on the right is the radiating antenna and LPDA on the left is the receiving antenna. On the right is the position of the phone with the phyphox app for adjusting the antenna to the right inclination.*

The measured vertical pattern deviates much stronger from the simulated pattern than the horizontal pattern (see Figure 6.12). The reason is that the vertical pattern is more influenced by the ground conditions and possible reflection or absorption of the ground material. Since the simulation is performed in free space the simulation and the measurement can not be compared satisfactorily. Ignoring the obvious kink at 330°, the basic pattern of the simulation is reproduced by the measurement. In the case of the measurement, the maximal vertical peak-to-peak voltage is 1.53(3) mV. The normalisation factor for the simulation is again unknown.

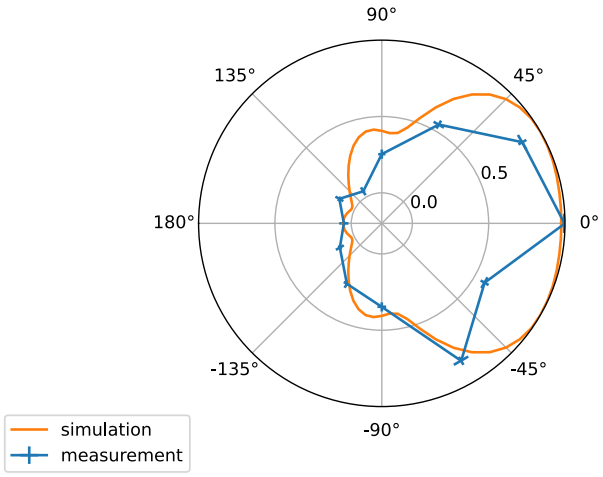

Figure 6.12: *Measured and simulated vertical linear gain radiation pattern, normalised to the radiation maximum. Simulation shows free space pattern. Measurement contains ground.*

6.4 Three LPDAs next to each other

The three antenna measurements were done at the distances of 2 m and 3 m, in order to see if the smallest or the regular distance between the antennas in the RNO-G experiment cause problems. Here the RNO-G configuration was used, meaning the middle antenna facing in one direction and the two outer antennas rotated by 120° outwards. The influence on one of the outer and the inner antenna was probed. These measurements were performed in free space (nearest wall at least 3.9 m away) and next to a wall. The wall measurements were done creating a reflecting surface 1.5 m away from the antennas in order to mimic the reflecting transition between ice and air above the antennas. Here the outer right antenna was probed, due to spacial reasons, explained in subsection 6.4.2. The free measurements were performed pointing the sending antenna directly towards the middle antenna (see subsection 6.4.1).

6.4.1 Three LPDAs in free space

As discussed in section 4.5, for the three-LPDA measurements in free space the RNO-G setup could be used. First a reference measurement with the setup with one LPDA (see Figure 6.1) was made. Then the two additional LPDAs were positioned in an 120° angle next to the receiving LPDA. One measurement is done with a spacing of $d_{\mathrm{LPDA}} = 2\,\mathrm{m}$ between the LPDAs and one measurement with $d_{\mathrm{LPDA}} = 3\,\mathrm{m}$ spacing.

Figure 6.13: *Photo of the measurement setup for the RNO-G three antenna setup in free space for* 3 m *spacing between LPDAs. The blue antenna on the right is the radiating antenna and the middle LPDA (center of the picture) is the receiving antenna.*

The biconical antenna sends its signal to the middle antenna, directly facing it. This leads to a cosmic ray-like situation, meaning the upward facing antenna receives a strong signal. This scenario was chosen to get, in case there is an effect, a symmetric effect from both disconnected antennas. Two different distances ($d_{\mathrm{re}} = 1.5\,\mathrm{m}$ and $d_{\mathrm{re}} = 1.8\,\mathrm{m}$) between emitter and receiver were probed, in order to test the reproducibility of the results. The emitting antenna was not moved while probing the different LPDA configurations to avoid corresponding systematic errors. Still it is possible that the $d_{\mathrm{LPDA}} = 2\,\mathrm{m}$ measurements are not that comparable, because they could not be conducted directly after each other, and therefore the antennas are possibly not in the exact same location in both measurements. It was decided that the systematic error of the distance between receiver and emitter was more important. The precision of the measurement was limited, due to measuring the different distances and angles by hand. Hence, it was tried to change as few parameters as possible during a measurement series. In addition, the statistical uncertainty of 0.03 mV (see subsection 6.2.2) has to be considered.

The waveforms of the different data sets and also the deviations look very similar to each other. For Figure 6.14 the deviations were calculated subtracting the three-antenna data set from the one-antenna data set. They were divided by the absolute maximum of the peak-to-peak voltage of the one-antenna data set in the signal region as a reference point, in order to get a percentage (see subsection 6.2.1). Note that these deviations correspond to a voltage that is a slightly higher than the statistical uncertainty of 0.03 mV. The range of the occurring signal is shaded in grey. Comparing this region to the noise, no difference is visible. The data set for $d_{\mathrm{re}} = 1.5\,\mathrm{m}$ and $d_{\mathrm{LPDA}} = 3\,\mathrm{m}$

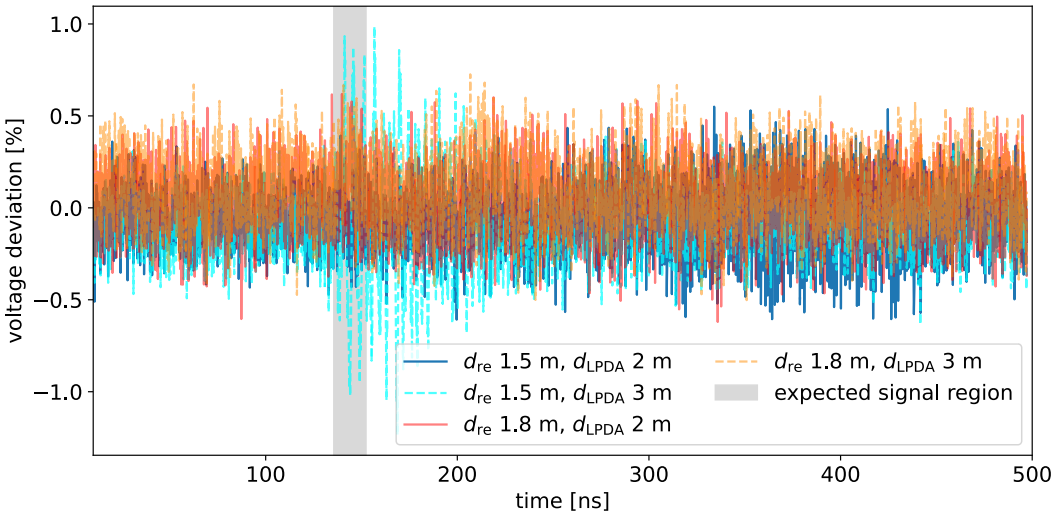

Figure 6.14: *Voltage amplitude deviations for the free space measurements in percent for two different distances between sending and receiving antenna (d_{re} in the legend) and two different distances between the three LPDAs (d_{LPDA} in the legend).*

starts to show a higher amplitude after the signal occurs, but the frequency does not match the frequency of the signal and is therefore not correlated. Since this effect is only visible in one of the four data sets, it might be possible that the upsampling changed the actual waveform too much. This leads to the conclusion that there is no noticeable effect of other antennas on the receiving antenna.

Looking at Table 6.2 the maximal deviations and the deviation ratios diminish[i]. The maximal absolute deviations in the signal region were calculated. The deviation ratios relates the signal deviation to the signal of the one-antenna measurement, meaning the amplitude deviation of the measurement $\Delta V(3, d_{re}, d_{LPDA})$ (see Equation 6.5) is divided by the one-antenna maximum peak-to-peak voltage $V_{pp}(1, d_{re}, d_{LPDA})$. The table shows that for the 3 m cases the deviation from the one-LPDA data set is larger than the 2 m configurations. This is true for both receiver-emitter distances, and therefore a statistical fluctuation can be excluded. Possible reasons for this behaviour could be resonances at this distance and frequency (400 MHz).

$$\Delta V(3, d_{re}, d_{LPDA}) = V(1, d_{re}, d_{LPDA}) - V(3, d_{re}, d_{LPDA}) \tag{6.5}$$

[i] calculations available on the RNO-G GitHub page in the LPDA_analysis repository

distance	maximal deviation [mV]		deviation ratio	
	2 m	3 m	2 m	3 m
1.5 m	0.07	0.16	0.004	0.010
1.8 m	0.07	0.08	0.006	0.007

Table 6.2: *Peak-to-peak voltage amplitude deviations for two different distances between sending and receiving antenna (left column) and two different distances between the three LPDAs (indicated in the second row). The maximal deviation in* mV *and the deviation ratio (maximal three-antenna deviation divided by one antenna signal) is displayed.*

Unfortunately a direct comparison to the simulation is impossible, due to the simulation normalisation. The highest gain point is normalised to 0 in the simulation, hence the one-antenna pattern and the three-antenna pattern both have the same value there. This leads to a deviation ratio of 0, which is not the case for the measurement deviation ratio. But using the Half-Power Beamwidth spectrum of simulation deviations, a rough comparison can be made. Therefore the vertical and the horizontal ratios are averaged. For the 2 m case the simulation predicts an effect of 1.15 %, which is higher than the measured effect. For the 3 m case a 0.3 % effect is predicted and is therefore lower than the measured effect. Both results do not agree with the measurements. A possible explanation is the influence of the floor in the measurements, which is missing in the simulation.

6.4.2 Three LPDAs near wall

For the wall measurements the spacial circumstances were difficult to realise, since an even wall without any cabinets was needed to represent the ice. This requirement was only fulfilled for a 2 m spacing setup and an extra wall next to it. Looking at Figure 6.15 the rightmost LPDA was probed, in order to be as far away from the walls as possible. Nevertheless the biconical antenna could not be placed directly in front of the receiving LPDA, because the cable was too short. A longer one would have changed the results compared to other measurements, because its different cable delay and was therefore depreciated. As for the free space measurements the distances 1.5 m and 1.8 m between receiver and emitter were probed, but in this case the antennas were placed at an angle of 60° to each other.

Figure 6.15: *Picture of the setup with three LPDAs next to the wall on the left. The blue antenna in the middle of the picture is the radiating antenna and the rightmost antenna is the receiving antenna. On the right the setup with one LPDA is shown.*

First the signal of a free space measurement and a wall measurement with 1.5 m between the receiver and emitter are compared. As displayed on the left in Figure 6.16 the wall signal is by a factor 9 smaller than the free space signal. This was expected since the LPDA is rotated to face the emitting biconical antenna at an angle of 60°, leading to a small signal. The small signal can be partially explained with the horizontal radiation pattern, discussed in section 6.3. The rotation should reduce the signal by approximately one half, the rest of the signal reduction seems to be due to the influence of the walls. In addition, the reflections from the wall can be seen. Compared to the free space measurement the signal near the wall is longer and contains two signals which seem to resemble the sent signal. The second signal is a reflection, similar to what was seen in the chamber measurements (remember section 5.3).

Now the results from one antenna and three antennas close to the wall are compared (see right side of Figure 6.16). In contrast to the free space measurement comparison between one and three antennas, for the near wall measurements the amplitude difference between the two data sets is visible. This leads to the conclusion that the wall enhances the effect of the disconnected antennas. Looking into the differences between the three- and the one-antenna signals a more detailed analysis is possible and will be done in the following.

The original deviations and the deviations after upsampling and shifting (same calculation as in subsection 6.4.1) show no major differences (see Figure 6.17). The shift amounted to 1/100 of the original sampling time of the oscilloscope for the 1.5 m case

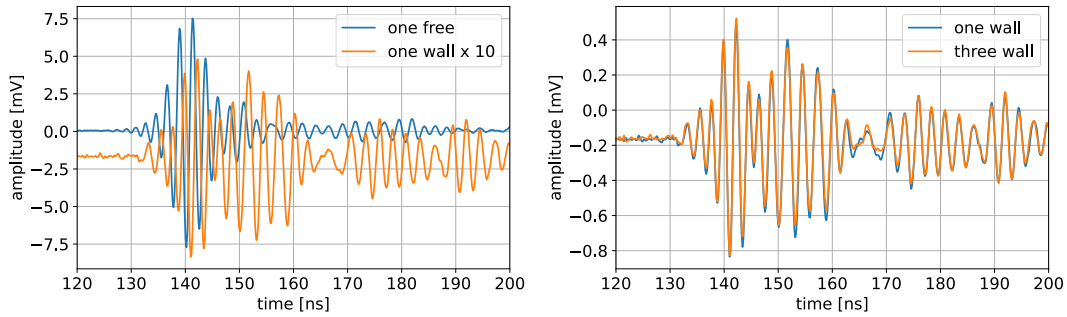

Figure 6.16: *On the left a* 1.5 m *measurement near the wall is compared to a free space measurement. Note that the wall measurement is enlarged by the factor* 10*, for better comparison. On the right side the wall measurements with one antenna and three antennas at* 1.5 m *are displayed.*

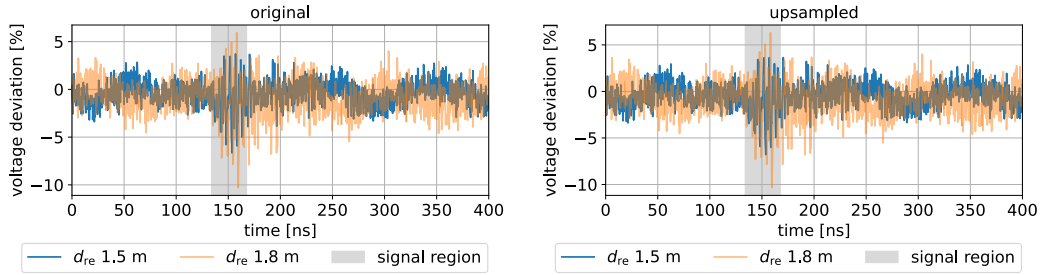

Figure 6.17: *Voltage amplitude deviations for the wall measurements in percent for two different distances between sending and receiving antenna (biconical distance in the legend). On the left side the original data are shown and on the right the upsampled and shifted data are presented.*

and none for the 1.8 m case. Therefore, the original signal was used for further analysis. The maximal voltage deviations were calculated to be 6.7 % in the 1.5 m case and 10.3 % in the 1.8 m case. A clear distinction between noise and signal deviation can be made. The seemingly sinusoidal behaviour of the noise is not understood, but present in both measurements and can therefore be categorised as unknown systematics. It is not certain, if this signal deviation effect is visible for the reflection on the ice surface. It is also not clear how much the second wall contributes to this effect.

Comparing the signal to the deviation for 1.8 m between emitter and receiver a correlation between the amplitudes of the one-antenna signal and the difference between one and three antennas can be seen. This is shown in Figure 6.18. For better visibility the signal offset of −0.17 mV was compensated. The correlation is visible

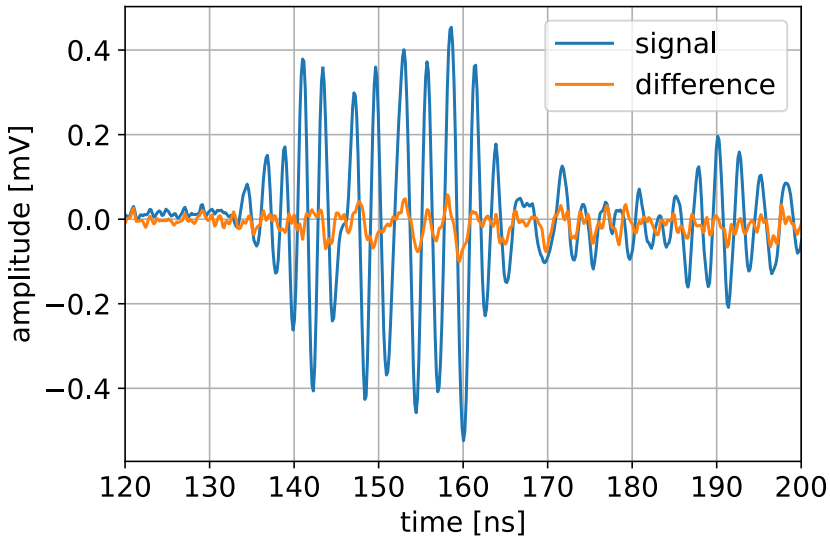

Figure 6.18: *Comparison of the* 1.8 m *one antenna signal and the difference between one and three antennas for this case. For better visibility the signal offset of* −0.17 mV *was compensated.*

for the reflected signal, meaning the part from 150 ns to 160 ns. Here the differences have the same frequency and phase as the signal. This leads to the conclusion that the one-antenna signal is stronger than the three-antenna signal. Hence the two disconnected antennas reduce the reflected signal. This is also visible on the right side of Figure 6.16. The same is true for the 1.5 m distance between emitter and receiver.

6.4.3 Result comparison to power calculation

In the previous sections the peak-to-peak voltage was used to quantify the effect of disconnected antennas next to a passive antenna. This method depends strongly on individual measurements that might be affected by digitisation effects or statistical effects. The signal power takes every feature of the signal into account and not just the maximum. Therefore, also the power P was considered and compared to the peak-to-peak voltage results.

In order to get the voltage V of the signal without noise contamination, the sample signal region defined in subsection 6.2.1 was used. In this region it was integrated over the squared voltage, where a possible voltage offset V_{off} was subtracted. This calculation, see Equation 6.6, results in the power of the signal.

$$P = \int_{\text{signal start}}^{\text{signal end}} (V - V_{\text{off}})^2 \tag{6.6}$$

For comparison to the percentage values in Table 6.2 the calculated power of the three-antenna signal was divided by the power of the one-antenna signal. The results of the comparison are displayed in Table 6.3.

For the free space measurements the voltage approach results in a positive effect on the amplitude of 1 % and below. The power method results show a negative effect in the sub percent regime. The deviation of both methods by approximately 1 % is considered to be within the uncertainties. This leads to the conclusion that the effect is very small and therefore negligible.

The wall measurement result for the two methods are in good agreement. Therefore it can be assumed that the effect is real and not only measured because of the measuring method.

The results do not deviate much from each other. The largest difference between the two methods is 1.8 %. Therefore the two methods are in good agreement.

	measurement		deviation	
location	d_{re} [m]	d_{LPDA} [m]	voltage [%]	power [%]
free space	1.5	2	0.4	−0.2
free space	1.5	3	1	−0.5
free space	1.8	2	0.6	−0.2
free space	1.8	3	0.7	−0.0
wall	1.5	2	6.7	7
wall	1.8	2	10.3	8.5

Table 6.3: *Comparison of the voltage and power deviations in percent. The measurement is described by its location, the distance between receiver and emitter d_{re} and the distance between the LPDAs d_{LPDA}.*

6.5 Experimental hall measurement results

First the signal received by the LPDA and the uncertainties were investigated. The statistical uncertainties were estimated to be 0.03 mV and the systematic uncertainties concerning the distance variation and time jitter of the oscilloscope were discussed.

With the one-antenna setup the horizontal and vertical radiation pattern were cross-checked with the simulation results. Even though not being in the far field the patterns

match the simulation quite well. The consequence would be that at a distance of two wavelength the far field is already well approximated.

Two antennas placed next to the antenna whose properties are investigated (three-antenna setup) in free space showed a very minor effect compared to the one-antenna signal. These sub percentage level deviations were not recognisable compared to the oscilloscope noise level. The effect of having three antennas at 2 m or 3 m distance to each other is also negligible.

The results for the three antennas near the wall show stronger deviations from the one-antenna setup. This suggest that the disconnected antennas reduce the reflected signal. It is however not clear if the effect of the wall is comparable to the properties of the ice and therefore act differently. Hence no clear statement about the effect expected in RNO-G can be made.

Possible improvements of the measurement technique In order to trace the radiation patterns better, one could measure the angles where the simulation showed interesting features. It would be advisable to always place the receiving antenna at the same distance between active element and emitting antenna and not just rotate the tripod. This would help to get a more accurate amplitude-angle relation.

7 Conclusion

The topic of this thesis was the investigation of a mutual influence of LPDA antennas placed at distances of 2 m to 3 m in RNO-G. The goal was to find possible signal disturbances produced by antennas in close proximity. This was achieved by studying the theory of LPDA antennas, simulating the antenna with the simulation tool 4nec2 and comparing it to measurements.

The theory (see subsection 3.3.2) predicts that the LPDA antenna has a strong beaming in forward direction. Therefore, the antennas in the RNO-G setup are arranged so that they face away from each other (see section 3.2), and are therefore sensitive in different directions. This should result in a minimal mutual interference of the antenna signal. Observation in the field could be interpreted as a stronger than expected mutual influence of the antennas.

The simulations show that there is a frequency and spacing dependence of the antenna radiation patterns (see section 4.4). Comparing the radiation pattern of a setup with two other antennas within close proximity to the radiation pattern of one antenna, differences are observable. The changes in the pattern become smaller the higher the frequency and the further apart the antennas are. These effects on the signal gain are in the order of 1 % for the vertical patterns and even smaller for the horizontal patterns. An exception to this rule is the 100 MHz case.

Measurements were first done in the RF chamber of the ECAP Laboratory, which turned out not to be usable for the investigation of this thesis. The true amplitude response of the antenna to a send signal could not be guaranteed in the chamber, because of interference from reflections at the chamber walls. Nevertheless using the results of the cable study (see section 5.2) the best suited frequency (400 MHz) was found. Investigating the transmission from the biconical antenna to the Vpol antenna, the best signal waveform (three-sine oscillation burst) could be derived.

In order to give a full and detailed answers to the main question of this thesis the experimental hall at the ECAP laboratory was chosen to conduct measurements. Here the signal was studied further, conducting a high statistics measurement to understand the representativeness of the following measurements. In addition mitigation strategies for systematical errors were found and applied to the following measurements. The measured radiation patterns fit quite well the expectations of the simulation, leading to the result that the simulation represent the reality fairly good. The measurements

performed with three antennas next to each other in free space showed little deviation from the one-antenna case. This result is in good agreement with the expectations from the simulation. The deviation results for the near wall measurements were more pronounced, but at the same time the setup does not represent reality well enough to be considered.

This all leads up to the conclusion that the LPDAs do not influence each other enough to change the current RNO-G setup. A slight effect on the receiving properties of the LPDA was predicted by the simulation, but could not be confirmed by the measurements. The effect found in the wall measurements is not large enough to disturb data taking in any way. There are still some open questions, like, whether the termination of the passive antennas changes the behaviour? Is the concrete wall in the experiment hall a good substitute for ice? These questions need to be addressed in future work.

A Station surface layout

In this section, the calculation of how far apart the LPDA antennas are in the field will be explained. The available RNO-G detector json data in NuRadioReco [28] was used to calculate the distances between two channels. The uncertainties for these distance measurements depend on the precision of the uncalibrated GPS data. The plotted layout for the three stations deployed in 2021 is depicted in Figure A.1. The position of the antenna feed point is given relative to the station position [29]. The distances of interest are those of the neighbouring antennas grouped together, e.g. for station 11 it is the distances between the channels 12 and 13, 13 and 14, 15 and 16, 16 and 17, and so on.

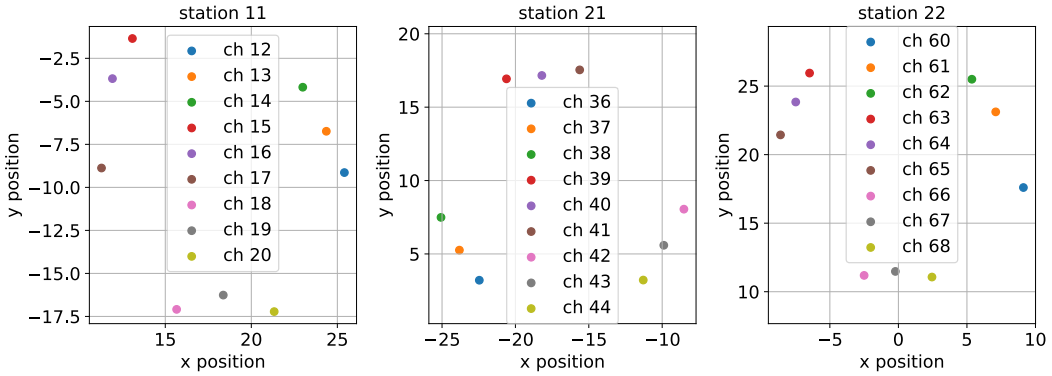

Figure A.1: *X- and y- positions of surface channels for the three stations deployed in 2021. The positions are displayed in meter.*

The minimal and maximal distance as well as the mean and standard difference for each station are listed in Table A.1. In the fourth row the parameters for all stations combined are shown. From the smallest total distance the conclusion is drawn to take measurements at a distance of 2 m as the lower bound and compare it with 3 m, which is the average distance.

	min	max	mean	std
station 11	2.62	5.23	3.22	0.92
station 21	2.42	2.81	2.6	0.14
station 22	2.3	5.88	3.13	1.25
total	2.3	5.88	2.99	0.77

Table A.1: *Calculated distances between neighbouring antennas for the three stations deployed in* 2021. *The table contains the minimal distance (min), the maximal distance (max), the mean distance (mean) and the standard difference of the mean (std) for each station and for all station (total) in one data set. All values are given in meter.*

B CLP5130-2 geometry

To create the antenna model, all dipole lengths and the distances between the dipoles had to be measured. For both measurements a measuring tape was used, therefore the error of all the measurements is estimated to be ±3 mm. The length measurement was prone to error, due to the height difference between the boom and the dipole. The difficulty for the distances was to find the centre of the dipoles to always have the same reference point.

For the dipole length (shown in Table B.1), the full length l_n was measured, i.e. both dipole halves left and right of the boom together. This quantity was used to calculate τ in Equation 3.3. The half lengths were needed for the model since the boom was constructed to lie on the zero point of the axis. In order to achieve this the full lengths were divided by 2.

Dipole number n	Full length [m]	Half length [m]
1	0.078	0.039
2	0.094	0.047
3	0.112	0.056
4	0.138	0.069
5	0.164	0.082
6	0.196	0.098
7	0.236	0.118
8	0.284	0.142
9	0.34	0.17
10	0.408	0.204
11	0.488	0.244
12	0.583	0.2915
13	0.704	0.352
14	0.848	0.424
15	1.014	0.507
16	1.21	0.605
17	1.45	0.725

Table B.1: *Measured dipole lengths in meter. Enumeration starts with the smallest dipole. The full lengths were measured and the half lengths were needed for the model.*

Also two types of distances were needed: the distance to the next dipole and the boom position, i.e. the distance from the smallest to the desired dipole. Both types are listed for all dipoles in Table B.2. The distances between the dipoles were used to calculate the numerator of the parameter σ in Equation 3.2. The boom position helped constructing the antenna model. The boom position was constructed by adding all distances to the next dipole up to the desired dipole.

Dipole number n	Distance to next dipole [m]	Boom position [m]
1	0.015	0
2	0.018	0.015
3	0.024	0.033
4	0.028	0.057
5	0.035	0.085
6	0.04	0.12
7	0.047	0.16
8	0.059	0.207
9	0.068	0.266
10	0.08	0.334
11	0.098	0.414
12	0.115	0.512
13	0.137	0.627
14	0.165	0.764
15	0.195	0.929
16	0.235	1.124
17	0	1.359

Table B.2: *Measured dipole distances in meter. Enumeration starts with the smallest dipole. The measured distance from the smaller to the bigger dipole is shown in the row of the smaller dipole.*

All measurements were done in meter, since it is the standard unit of 4nec2. The dipole enumeration starts with the smallest dipole. From these measurements and the calculated τ and σ (see subsection 4.2.1) as input, a website [21] could calculate all design parameters. The input and the result of these calculations can be found on the next two pages. They are similar to the results obtained by the measurements. Note that the web page starts the numeration with the biggest dipole. The only value used form this source is the "Required characteristic impedance of the feeder connecting the elements Zc_feed" given in the last row of the second page.

LPDA — https://hamwaves.com/lpda/ — v20180914
LPDA design 2022-10-13 13:47

INPUT
Lowest frequency f_1 = 105 MHz
Highest frequency f_n = 1300 MHz
Diameter of the shortest element ⌀ = 4 mm
Characteristic input impedance Zc_in = 50 Ω
Taper τ = 0.833
Optimal relative spacing σ_{opt} = 0.151
Chosen relative spacing σ = 0.083

RESULTING DESIGN
Number of elements ⌊N⌉ = 17
Dipole element lengths:
dipole ℓ_1 = 1.428 m
dipole ℓ_2 = 1.189 m
dipole ℓ_3 = 0.991 m
dipole ℓ_4 = 0.825 m
dipole ℓ_5 = 0.687 m
dipole ℓ_6 = 0.573 m
dipole ℓ_7 = 0.477 m
dipole ℓ_8 = 0.397 m
dipole ℓ_9 = 0.331 m
dipole ℓ_{10} = 0.276 m
dipole ℓ_{11} = 0.230 m
dipole ℓ_{12} = 0.191 m
dipole ℓ_{13} = 0.159 m
dipole ℓ_{14} = 0.133 m
dipole ℓ_{15} = 0.111 m
dipole ℓ_{16} = 0.092 m
dipole ℓ_{17} = 0.077 m
Sum of all dipole lengths ℓ_{tot} = 8.166 m

Distances between the element centres
and their position along the boom:
$d_{1,2}$ = 0.237 m, i.e. ℓ_2 @ 0.237 m
$d_{2,3}$ = 0.197 m, i.e. ℓ_3 @ 0.434 m
$d_{3,4}$ = 0.164 m, i.e. ℓ_4 @ 0.599 m
$d_{4,5}$ = 0.137 m, i.e. ℓ_5 @ 0.736 m
$d_{5,6}$ = 0.114 m, i.e. ℓ_6 @ 0.850 m
$d_{6,7}$ = 0.095 m, i.e. ℓ_7 @ 0.945 m
$d_{7,8}$ = 0.079 m, i.e. ℓ_8 @ 1.024 m
$d_{8,9}$ = 0.066 m, i.e. ℓ_9 @ 1.090 m
$d_{9,10}$ = 0.055 m, i.e. ℓ_{10} @ 1.145 m
$d_{10,11}$ = 0.046 m, i.e. ℓ_{11} @ 1.191 m
$d_{11,12}$ = 0.038 m, i.e. ℓ_{12} @ 1.229 m
$d_{12,13}$ = 0.032 m, i.e. ℓ_{13} @ 1.261 m
$d_{13,14}$ = 0.026 m, i.e. ℓ_{14} @ 1.287 m
$d_{14,15}$ = 0.022 m, i.e. ℓ_{15} @ 1.309 m

$d_{15,16}$ = 0.018 m, i.e. ℓ_{16} @ 1.327 m
$d_{16,17}$ = 0.015 m, i.e. ℓ_{17} @ 1.343 m
Boom length L = 1.343 m

Length of the terminating stub ℓ_Zterm = 0.357 m
Required characteristic impedance of the feeder connecting the elements Zc_feed = 105.1 Ω

C Complete three antenna simulation data set

In this appendix most of the simulation results can be found in an overview plot (see Figure C.1). Both linear and logarithmic results are shown. Here one can see that in the logarithmic scale the negligible back lobe discrepancies are better visible than the important main lobe differences. The later are better visible in the linear patterns.

All the difference plots can be found in Figure C.2 as well. These were not plotted in a polar plot, but in a planar plot in order to see the differences in differences around the pattern. The differences ($D(o)$) were calculated subtracting the pattern for three antennas ($P(3, o)$) from the pattern for one antenna ($P(1, o)$), see Equation C.1 where the o parameter refers to the vertical or horizontal orientation. In order to mark the relevant regions of the patterns the Half-Power Beamwidth (HPBW) and the First-Null Beamwidth (FNBW) were used.

$$D(o) = P(1, o) - P(3, o) \tag{C.1}$$

For better comparison (see Figure 4.10), the extrema of these differences were calculated. Minima and maxima of the difference from the 3 m spacing three antenna simulation data set in the HPBW range can be found in Table C.1. The range from maximum to minimum is calculated subtracting the minimum from the maximum.

frequency	100 MHz	400 MHz	800 MHz	1200 MHz
max horizontal	0.35	0.02	0.02	0.01
min horizontal	−0.11	−0.03	−0.02	−0.02
range horizontal	0.46	0.05	0.04	0.03
max vertical	0.10	0.01	0.01	0.01
min vertical	−0.01	0.00	−0.02	−0.01
range vertical	0.11	0.01	0.03	0.02

Table C.1: *Minima and maxima of the difference from the* 3 m *spacing three antenna simulation data set in the HPBW range. The range from maximum to minimum is calculated subtracting the minimum from the maximum. All values are given in* dB.

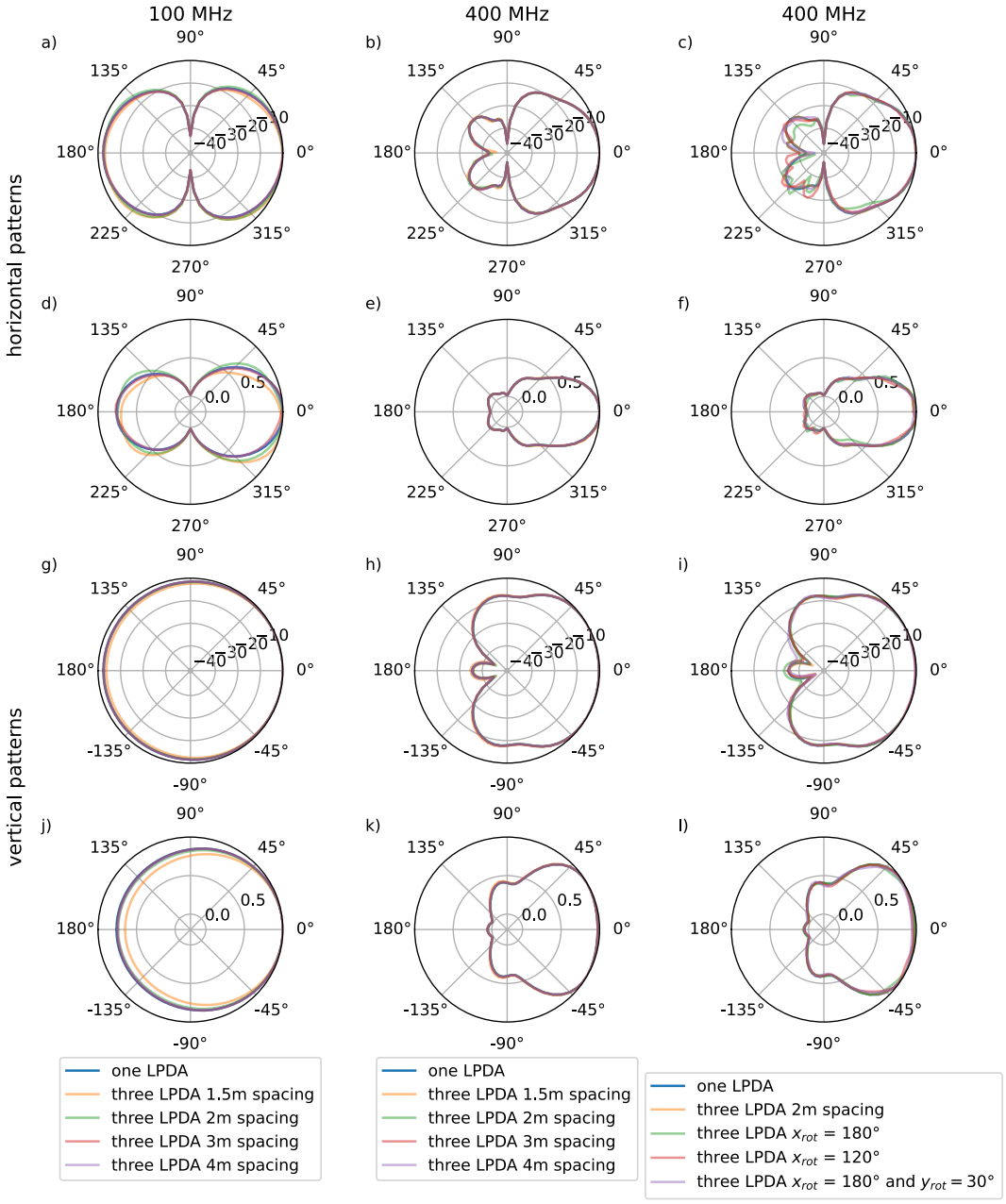

Figure C.1: *Radiation patterns for simulations with one active antenna on the left and two passive antennas to the right. First row are horizontal patterns in* dB*, the second contains linear horizontal patterns. The third and fourth row show the vertical patterns, respectively. One column contains one data set with its legend at the bottom: the left column describes the* 100 MHz *spacing simulations, in the middle the* 400 MHz *spacing simulations are shown and on the right are the results of the* 400 MHz *rotation simulations.*

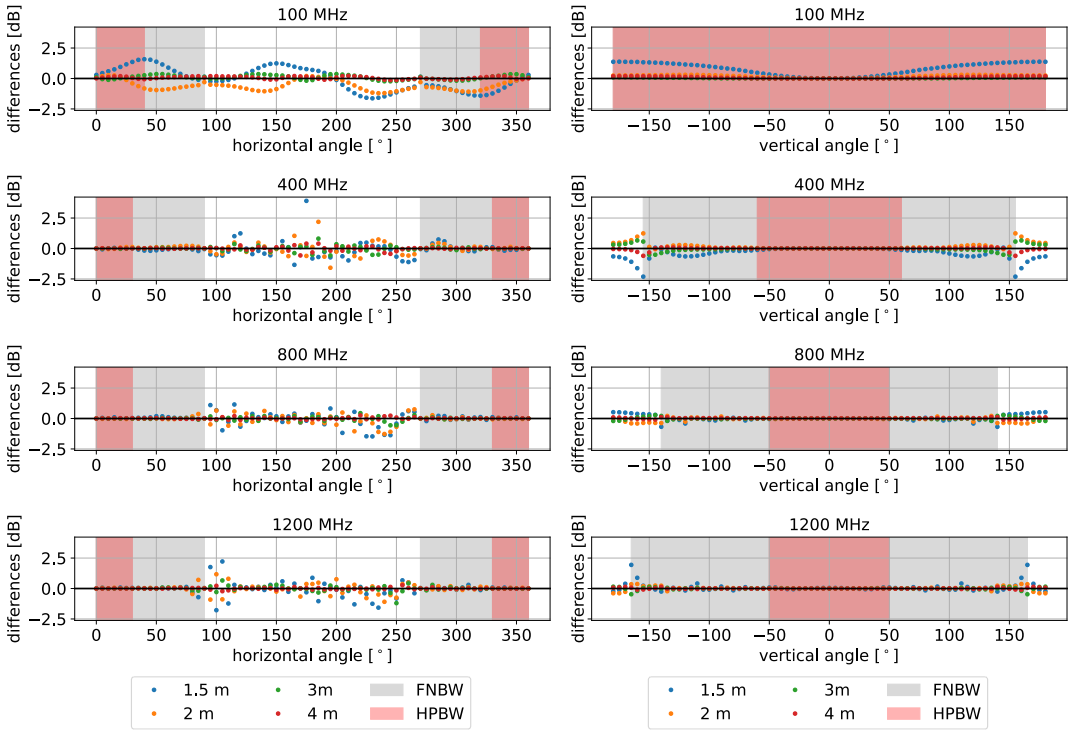

Figure C.2: *Differences for* dB *simulations with one active antenna on the left and two passive antennas to the right. The first column displays the horizontal pattern and the second the vertical pattern. Each row contains the four distance data sets at another frequency. The grey area marks the region of the FNBW and the red area is designated to the HPBW of the one antenna data set.*

D Cable reflection peaks for different frequencies

Here the analysis of the cable reflection at different frequencies gets explained more in detail. In order to find the peak positions the `scipy.signal` function `find_peaks` was used. The findings of that function can be seen in Figure D.1, Figure D.2 and Figure D.3. As can be seen there is a slight overshoot concerning the number of peaks, but this was needed to also find maximums in the last cluster of peaks (see Figure D.3). Even with the requirement of a prominence of 0.005 V and a height of 0.005 V the algorithm was not able to find peaks for 400 MHz and 500 MHz in the time frame where the third peak was suspected. On the other hand this also means that there might not be a third peak. Still some unwanted bigger peaks had to be sorted out by hand. The peak position results are listed in Table D.1.

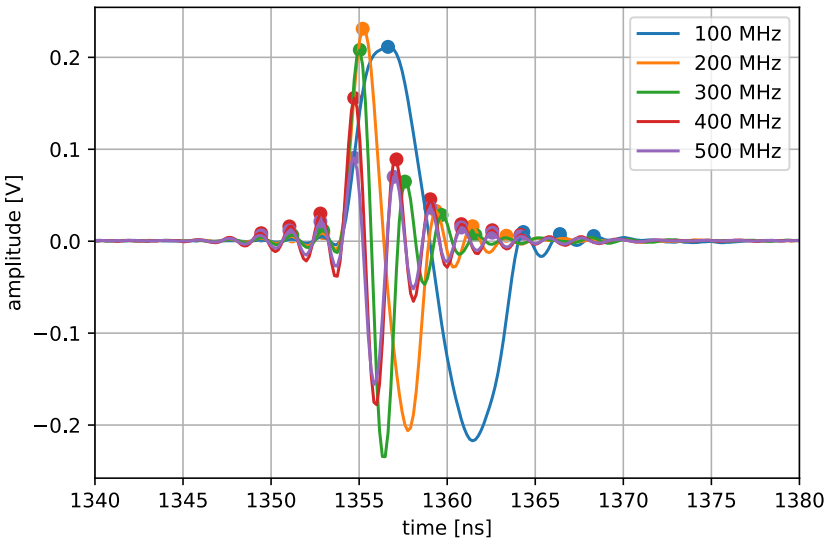

Figure D.1: *First cluster of peaks for frequency dependence of the input signal reflection. The dots denote the peaks found by the* `scipy` *function* `find_peaks`*.*

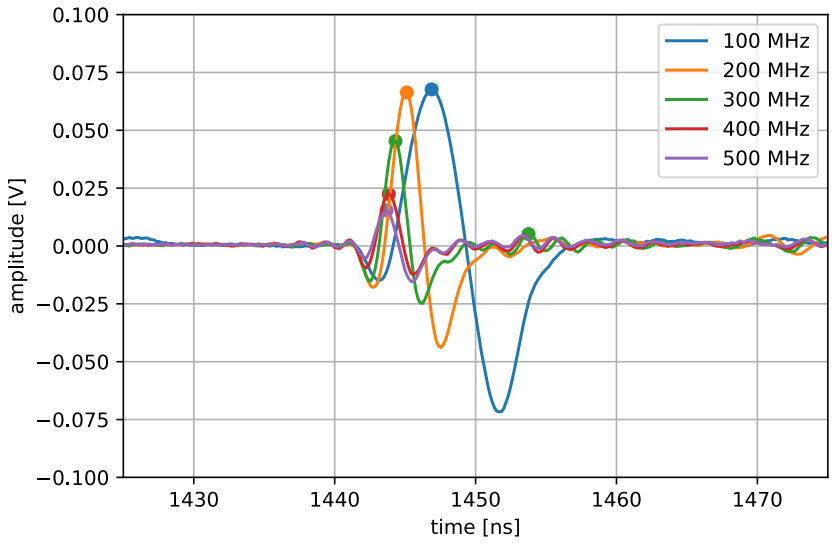

Figure D.2: *Second cluster of peaks for frequency dependence of the input signal reflection. The dots denote the peaks found by the* `scipy` *function* `find_peaks`*.*

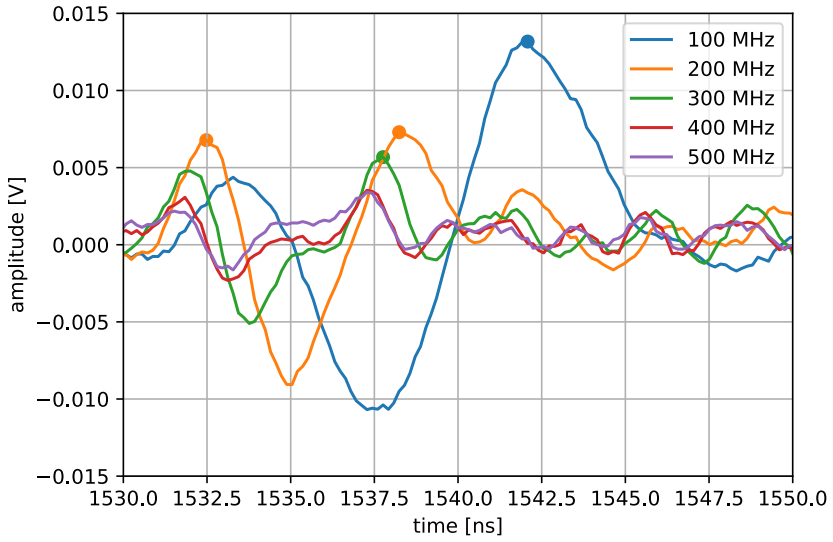

Figure D.3: *Third cluster of peaks for frequency dependence of the input signal reflection. The dots denote the peaks found by the* `scipy` *function* `find_peaks`*.*

	frequency	100 MHz	200 MHz	300 MHz	400 MHz	500 MHz
peak 1	height [V]	0.21	0.23	0.21	0.16	0.09
	time [µs]	1.356	1.355	1.355	1.355	1.355
peak 2	height [V]	0.068	0.066	0.045	0.022	0.015
	time [µs]	1.447	1.445	1.444	1.444	1.444
peak 3	height [V]	0.013	0.007	0.006	0	0
	time [µs]	1.542	1.538	1.538	0	0

Table D.1: *Peak position (signal height and time) of frequency dependent reflections (see dots in figures above) in the input signal of the function generator generated signal for the biconical antenna.*

Bibliography

[1] S. Fukuda et al. 'The Super-Kamiokande detector'. In: *Nuclear Instruments and Methods in Physics Research Section A: Accelerators, Spectrometers, Detectors and Associated Equipment* 501.2 (2003), pp. 418–462. ISSN: 0168-9002. DOI: https://doi.org/10.1016/S0168-9002(03)00425-X. URL: https://www.sciencedirect.com/science/article/pii/S016890020300425X.

[2] S. Adrián-Martínez et al. 'Letter of intent for KM3NeT 2.0'. In: *Journal of Physics G: Nuclear and Particle Physics* 43.8 (June 2016), p. 084001. DOI: 10.1088/0954-3899/43/8/084001. URL: https://dx.doi.org/10.1088/0954-3899/43/8/084001.

[3] M. G. Aartsen et al. 'IceCube-Gen2: the window to the extreme Universe'. In: *Journal of Physics G: Nuclear and Particle Physics* 48.6 (Apr. 2021). DOI: 10.1088/1361-6471/abbd48.

[4] A. Anker et al. 'Targeting ultra-high energy neutrinos with the ARIANNA experiment'. In: *Advances in Space Research* 64.12 (2019). Advances in Cosmic-Ray Astrophysics and Related Areas, pp. 2595–2609. ISSN: 0273-1177. DOI: https://doi.org/10.1016/j.asr.2019.06.016. URL: https://www.sciencedirect.com/science/article/pii/S0273117719304326.

[5] P. Allison et al. 'Design and Initial Performance of the Askaryan Radio Array Prototype EeV Neutrino Detector at the South Pole'. In: (Aug. 2011). DOI: https://doi.org/10.48550/arXiv.1105.2854.

[6] P. Schellart et al. 'Detecting cosmic rays with the LOFAR radio telescope'. In: *Astronomy & Astrophysics* 560 (Dec. 2013). DOI: 10.1051/0004-6361/201322683.

[7] A. Anker et al. 'Neutrino vertex reconstruction with in-ice radio detectors using surface reflections and implications for the neutrino energy resolution'. In: *Journal of Cosmology and Astroparticle Physics* 2019.11 (Nov. 2019), pp. 030–030. DOI: 10.1088/1475-7516/2019/11/030.

[8] M. Krause. 'Calibration of the LOFAR Antennas'. MA thesis. Radboud University Nijmegen, 2013.

[9] G.J. Burke and A.J. Poggio. 'Part I: Program description - Theory'. In: *Numerical electromagnetics code (NEC) - Method of Moments*. Lawrence Livermore Laboratory, Jan. 1981.

[10] C. A. Balanis. 'Antenna Theory: Analysis and Design'. In: 3rd ed. Hoboken, New Jersey: John Wiley & Sons, 2005. ISBN: 0-471-66782-X.

[11] IEEE. 'IEEE Standard for Definitions of Terms for Antennas'. In: *IEEE Std 145-2013 (Revision of IEEE Std 145-1993)* (2014), pp. 1–50. DOI: 10.1109/IEEESTD.2014.6758443.

[12] R. Krause. 'Antenna Development and Calibration for Measurements of Radio Emission from Extensive Air Showers at the Pierre Auger Observatory'. PhD thesis. RWTH Aachen University, 2018.

[13] J.A. Aguilar et al. 'Design and sensitivity of the Radio Neutrino Observatory in Greenland (RNO-G)'. In: *Journal of Instrumentation* 16.03 (Mar. 2021). DOI: 10.1088/1748-0221/16/03/p03025.

[14] G. Askaryan. 'Excess negative charge of an electron-photon shower and its coherent radio emission'. In: *Soviet Physics JETP* 14.2 (Feb. 1962), pp. 441–443. URL: https://inspirehep.net/files/50aa3b9f4a1271a1476462d1635d96a7.

[15] RNO-G collaboration. *Wiki for the Greenland radio detector collaboration*. [internal wiki page].

[16] D. Smith and RNO-G collaboration. *Wiki for the Greenland radio detector collaboration. Downhole V-Pol Antenna*. [internal wiki page].

[17] B. Hendricks on behalf of RNO-G collaboration. 'RNO-G Technical Review. Downhole antennas'. [internal talks]. Mar. 2023.

[18] D. Isbell. 'Log periodic dipole arrays'. In: *IRE Transactions on Antennas and Propagation* 8.3 (1960), pp. 260–267. DOI: 10.1109/TAP.1960.1144848.

[19] Creative Design Corp. *Instruction Manual CLP5130-2 Radio Antennas*. Japan, 1994.

[20] A. Rohatgi. *WebPlotDigitizer - Web Based Plot Digitizer*. [Last accessed 28 September 2022]. 2010-2022. URL: https://apps.automeris.io/wpd/.

[21] S. Stroobandt and M. McCue. *Log-Periodic Dipole Array Calculator*. [Last accessed 13 October 2022]. 2014–2020. URL: https://hamwaves.com/lpda/en/index.html.

[22] AARONIA AG. *Biconical antennas BicoLOG series*. Germany, 2022.

[23] Schirmung 2000. *Die neue Raumschirmungstechnologie*. Germany, 2005.

[24] Schirmung 2000. *Abschirmvlies*. [Last accessed 9 December 2022]. Germany, 2022. URL: https://www.schirmung2000.de/index.php?seite=abschirmvlies.

[25] W. R. Leo. *Techniques for Nuclear and Particle Physics Experiments*. 2nd ed. Berlin: Springer-Verlag, 1994. ISBN: 3-540-57280-5.

[26] Rollei. *C6i - Carbon Stativ*. [Last accessed 1 March 2023]. Germany, 2023. URL: https://www.rollei.de/products/carbon-stativ-c6i-22611#technische-daten.

[27] S Staacks et al. 'Advanced tools for smartphone-based experiments: phyphox'. In: *Physics Education* 53.4 (May 2018), p. 045009. DOI: 10.1088/1361-6552/aac05e.

[28] C. Glaser et al. 'NuRadioReco: a reconstruction framework for radio neutrino detectors'. In: *The European Physical Journal C* 79.6 (June 2019). DOI: 10.1140/epjc/s10052-019-6971-5.

[29] The NuRadio group. *NuRadio documentation. Properties of Detector Description*. [Last accessed 27 March 2023]. 2023. URL: https://nu-radio.github.io/NuRadioMC/NuRadioReco/pages/detector/detector_database_fields.html.

Acknowledgements

Many thanks to Anna and Robert for supervising me, giving me insight into the RNO-G collaboration and how to work in such a research environment. Thanks to the RNO-G group in Erlangen and Zeuthen for the support with small problems, once solved making life so much easier. Special thanks to Ugo for the help getting me started working with the simulation software and Adrian for helping me with all kinds of technical details. I also want to thank my family and friends for moral support and letting me explain stuff to understand it. Thanks to all the volunteers, prove reading my thesis and giving me much appreciated feedback.

Eigenständigkeitserklärung

Hiermit versichere ich, dass ich die vorliegende Masterarbeit selbstständig verfasst habe. Ich versichere, dass ich keine anderen als die angegebenen Quellen benutzt und alle wörtlich oder sinngemäß aus anderen Werken übernommenen Aussagen als solche gekennzeichnet habe, und dass die eingereichte Arbeit weder vollständig noch in wesentlichen Teilen Gegenstand eines anderen Prüfungsverfahren gewesen ist.

Erlangen, 15.5.2023 **Anna Eimer**